scientific reports

Check for updates

OPEN

Impacts of urbanization on energy balance in a central Amazonia city

Denisi Holanda Hall[1], Luiz Antonio Candido[1], Bruno Takeshi Tanaka Portela[1], Gilberto Fisch[2], Rita Valéria Andreoli[3], Rodrigo Augusto Ferreira Souza[3], Adam Stapleton[7], Alacimar Viana Guedes[1], Anne Cristiny Santos de Mendonça[1], Carla de Souza Farias[1], Jailson Ramos da Mata[8], Joice de Jesus Machado[4], Marcelo Crestani Mota[5], Maria Juliana de Melo Monte[1], Ranyelli Cunha de Figueiredo[1], Regison da Costa de Oliveira[1], Thiago de Lima Xavier[8] & Cléo Quaresma Dias-Júnior[1,6]✉

We investigate the components of radiation and energy balance and heat storage flux in an urban area of Central Amazonia, during the wet and dry seasons of 2022. Detailed radiation and turbulent energy fluxes measurements were conducted using a 30-meter micrometeorological tower. The analyses include an assessment of the energy balance closure, incorporating the urban canopy heat storage term. The main findings were: (i) A footprint analysis showed that during the wet season, the primary energy flux sources were from the impermeable surfaces, while in the dry season, in addition to impermeable surfaces, green areas also influenced the fluxes; (ii) Incoming shortwave radiation was significantly higher during the dry season; (iii) Albedo was higher in dry season compared to the wet season; (iv) Latent heat flux showed low sensitivity to seasonal variability, compared to sensible heat flux; (v) Energy balance closure significantly improved with the inclusion of urban canopy heat storage and soil heat flux, highlighting their critical roles in reducing energy imbalances. The measurements presented in this study are the first Eddy Covariance measurements for an urban region of the Amazon. These results are important for urban climate modeling in tropical regions, providing insights into the impacts of urbanization in the Amazon region.

Keywords Amazon region, Urban climate, Energy balance closure, Heat storage, Eddy covariance measurements

Urban centers play a crucial role in global climate change, as cities increasingly accommodate the world's population in a rural-to-urban migration flow. Approximately two-thirds of the global population will reside in cities by 2050[1,2]. Although cities occupy less than 3% of the Earth's surface, they consume 78% of the world's energy and generate over 60% of global greenhouse gas emissions[3].

The urbanization process drastically alters the radiative, thermal, hydrological, and aerodynamic properties of the surface[4–6]. These modifications directly impact surface-atmosphere interactions, altering the exchange of energy, momentum, and mass between them, leading to complex and poorly understood microclimates[7,8]. The surface energy balance is the physical process responsible for the coupling between the surface and the Atmospheric Boundary Layer (ABL). In urban areas, the partitioning of the energy balance between sensible and latent heat is significantly altered compared to rural/natural environments due to surface properties (3D geometry, roughness, impermeability of surface coverings, anthropogenic heat emissions, etc.) and complex distributions of heat sources/sinks[9]. Improving our understanding of energy exchanges in urban environments can lead to advancements in mitigating these impacts and provide guiding insights for risk management in these areas. Climate and weather forecasts for large cities (megacities), can also be improved by incorporating these findings.

In recent decades, several studies have used the Eddy Covariance (EC) method[10–12] to provide critical insights into the energy balance characteristics of urban surfaces[13–19]. Examples of studies in large cities such

[1]Graduate Program in Climate and Environment (CLIAMB), National Institute for Amazonian Research, Manaus, AM, Brazil. [2]University of Taubaté (UNITAU), Taubaté, SP, Brazil. [3]School of Technology (EST), Amazonas State University (UEA), Manaus, AM, Brazil. [4]Federal Institute of Education, Science and Technology of Amazonas (IFAM), Manaus, AM, Brazil. [5]Agronomy Coordination, Marechal Rondon College (FARON), Vilhena, RO, Brazil. [6]Department of Physics, Federal Institute of Education, Science and Technology of Pará (IFPA), Belém, PA, Brazil. [7]School of Computing, Dublin City University, Dublin, Leinster, Ireland. [8]Large-Scale Biosphere–Atmosphere Program in Amazonia (LBA), National Institute for Amazonian Research (INPA), Manaus, AM, Brazil. ✉email: cleo.quaresma@ifpa.edu.br

as Tokyo[16] and São Paulo[17] highlight variations in latent heat flux and energy storage, while research in Hong Kong[19] explores the relationship between surface heterogeneity and energy balance closure. In Beijing, Miao et al.[20] observed that nocturnal sensible heat flux is nearly zero on clear-sky days, whereas latent heat flux remains positive. However, on cloudy days, sensible nocturnal heat flux slightly exceeds latent heat flux during winter, with upward nocturnal heat flux primarily attributed to anthropogenic heat release.

However, few studies address the energy balance in tropical cities, where water availability plays a crucial role in energy flux dynamics. In Singapore, Roth et al.[18] observed that energy partitioning follows patterns similar to those of suburban regions in mid-latitudes, with the ratio of sensible heat to net radiation (H/Rn) and latent heat to the net radiation (LE/Rn) are approximately 53% and 40%, respectively. The scarcity of data in tropical regions underscores the need for more research to understand how the climatic and urban characteristics of these areas, combined with the availability of water, influence the balance of energy in cities.

In the largest tropical rainforest region in the world, fundamental studies on energy balance dynamics began with pioneering eddy covariance observations at the Ducke Reserve in the early 1980s[21–24]. These early campaigns laid the baseline for subsequent field experiments in forest and pasture areas, yielding crucial insights into energy partitioning, carbon cycling, and surface–atmosphere interactions[25–33]. For example, von Randow et al.[29] compared measurements of radiation, energy, and CO2 fluxes between forest and pasture regions in southwestern Amazonia, enhancing the understanding of differences in radiation and energy balance between forest and pasture land cover. They found that the most significant changes occurred in reflected shortwave radiation, which increased from $26.1\,Wm^{-2}$ in forest to $40.6\,Wm^{-2}$ in pasture (55% increase). They also observed that the sensible and latent heat flux above the pasture was higher and lower, respectively compared to the forest. It is known that an increase in sensible heat flux affects the dynamics of the convective boundary layer, making it deeper above the pasture, especially during the dry season[34–36]. However, most atmospheric turbulent flux measurements in the Amazon region have been conducted in rural and/or natural areas, and the dynamics of surface-atmosphere exchanges in densely urbanized areas remains unknown.

The city of Manaus, located in Central Amazonia, is the largest city in the Brazilian Amazon region and has seen its population more than triple since the 1980s, growing from 642,000 to approximately 2.2 million inhabitants[37,38] One of the first studies on Manaus, employing a comparative approach among forest, pasture and urban sites, using in situ data (i.e. air temperature, relative humidity, and evaporation), was conducted in the 1990s[39]. Since then, Manaus has been relatively underexplored in terms of scientific experiments focused on the impact of urban surfaces on the local climate. The intense urbanization process, coupled with population growth, has negatively affected the urban microclimate[40–42]. These impacts include surface warming[43–46] and, consequently, warming of the air layer in direct contact with the surface[40,41], driven primarily by anthropogenic heat[47]. Urban surfaces are known to interact with the atmosphere differently than natural surfaces. Hall et al.[48] in a preliminary study, used 3 months of data measured in the transition period from dry to rainy season in the city of Manaus and observed that sensible heat fluxes increased and latent fluxes were very close to those measured in a primary forest $150\,\mathrm{km}$ from Manaus.

Another significant impact is air pollution, which reduces incident solar radiation due to the emission of particles and gases. For instance, anthropogenic nitrogen oxide emissions in Manaus intensify the formation of secondary organic aerosols, which can be transported up to $150 - 200\,\mathrm{km}$ in the prevailing wind direction[49]. Therefore, the effects of urbanization in Manaus extend beyond the local scale, with relevant implications at the mesoscale. This diversity of impacts makes it crucial to investigate how city-atmosphere interactions are modified on a seasonal scale.

This study represents a pioneering investigation into the energy balance of urban areas in Manaus. It provides a significant contribution to the understanding of energy balance in tropical urban megacities. Furthermore, a comparative study of the components of the energy balance above Manaus in relation to the forest surrounding it and in relation to other tropical and subtropical cities is carried out. With this we have a better understanding of the effect of urbanization on the energy partition in the Amazon region.

Data and methods

Site description and instrumentation

The experimental data used in this study were collected in the urban center of Manaus, Amazonas, Brazil ($03°07'02''$ S, $59°59'57''$ W; 92 m above sea level) (Fig. 1 a). Manaus is located in the central Amazon region and currently covers an estimated area of $11,401\,\mathrm{km}^2$. According to data from the MapBiomas project[50], the land use and land cover in the urban area are predominantly classified as urban (48%), followed by forest fragments (35.5%), agriculture (11.8%), and other land cover classes each comprising less than 4% (Fig. 1a).

The experimental site of the Urban Micrometeorological Tower (named as TURB) is located in a high-density residential area of Manaus (Fig. 1b), specifically in the Petrópolis neighborhood in the southern-central zone of the city. The neighborhood is primarily residential, characterized by irregular terrain and steep topographic elevations, and consists of a mix of residential buildings and clusters of houses typical of Brazilian urban peripheries, with the average building height is approximately 8-10 meters, typically corresponding to 2 to 3 stories. Within a 500-meter radius of the tower, the surface is 80.5% impermeable surfaces (buildings and impermeable surfaces) and 19.5% permeable surfaces (vegetation, soil and river), as illustrated in Fig. 1b. Figure 1c illustrates the surface heterogeneity, which varies by the wind direction. Permeable fractions range from 9 to 31%, being higher in the SW (31.5%), S (26.5%), and W (26%) sectors due to the presence of vegetation along an extensive watercourse and tree-lined streets, with isolated vegetation. In contrast, the E sector features predominantly impermeable surfaces, reaching up to 91% impermeability.

The data were collected from a 30-meter micrometeorological tower located within the premises of the Amazonas Military Fire Department Headquarters (Fig. 2). The instruments installed and the variables measured on the tower are detailed in Table 1. The Eddy Covariance (EC) system was mounted at the top of the tower,

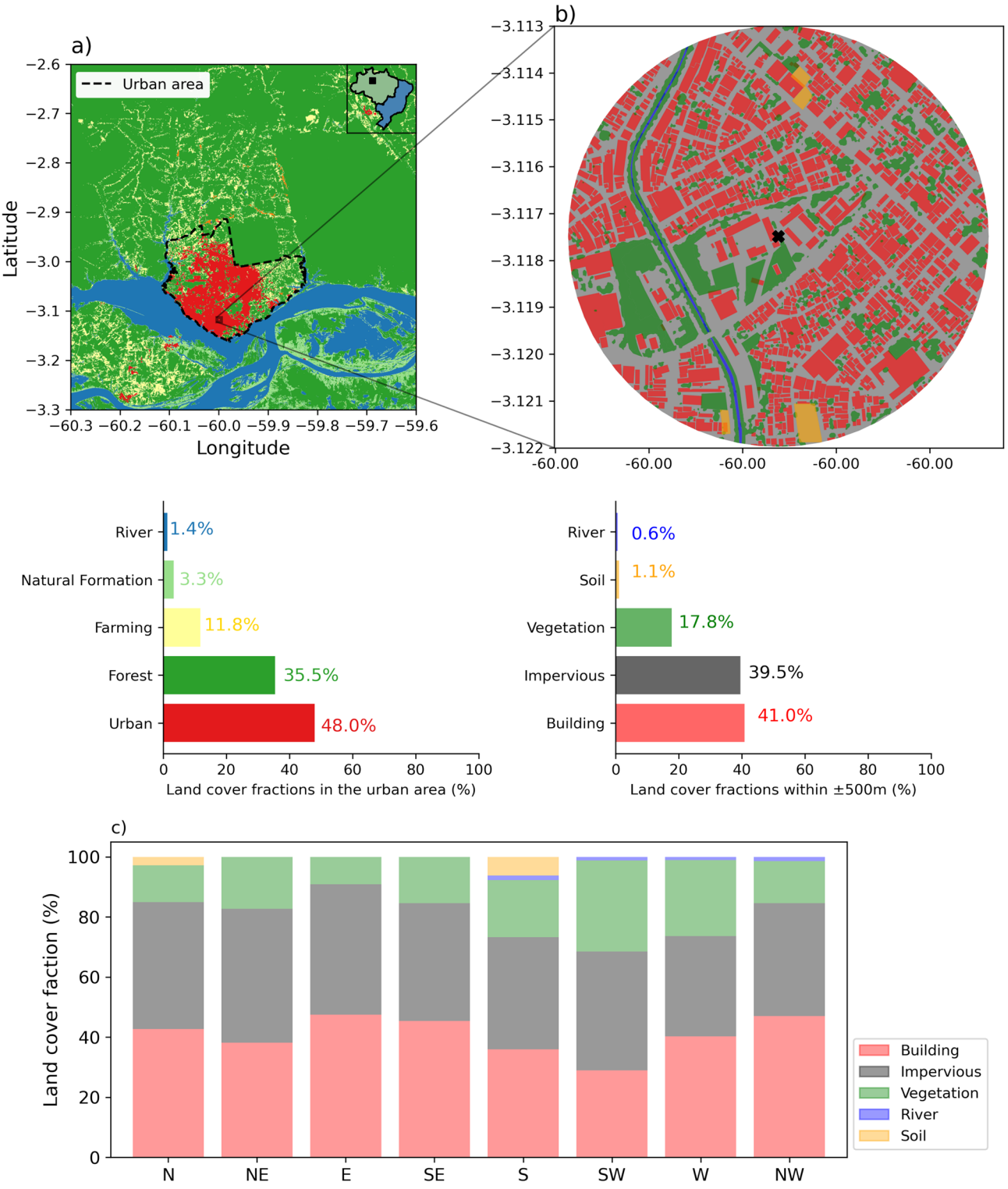

Fig. 1. (**a**) Geographic location and land use and land cover in the city of Manaus, data from MapBiomas (2022)[5150]. (**b**) Land cover and land use within a radius ±500 m of the TURB flux tower (black symbol in the center). (**c**) Land cover fractions within a radius ±500 m in relation to the cardinal directions (N: North, NE: Northeast, E: East, SE: Southeast, S: South, SW: Southwest, W: West, NW: Northwest). Impermeable surfaces include parking lots and other surfaces covered by concrete or asphalt. Maps generated in Python v3.12.7.

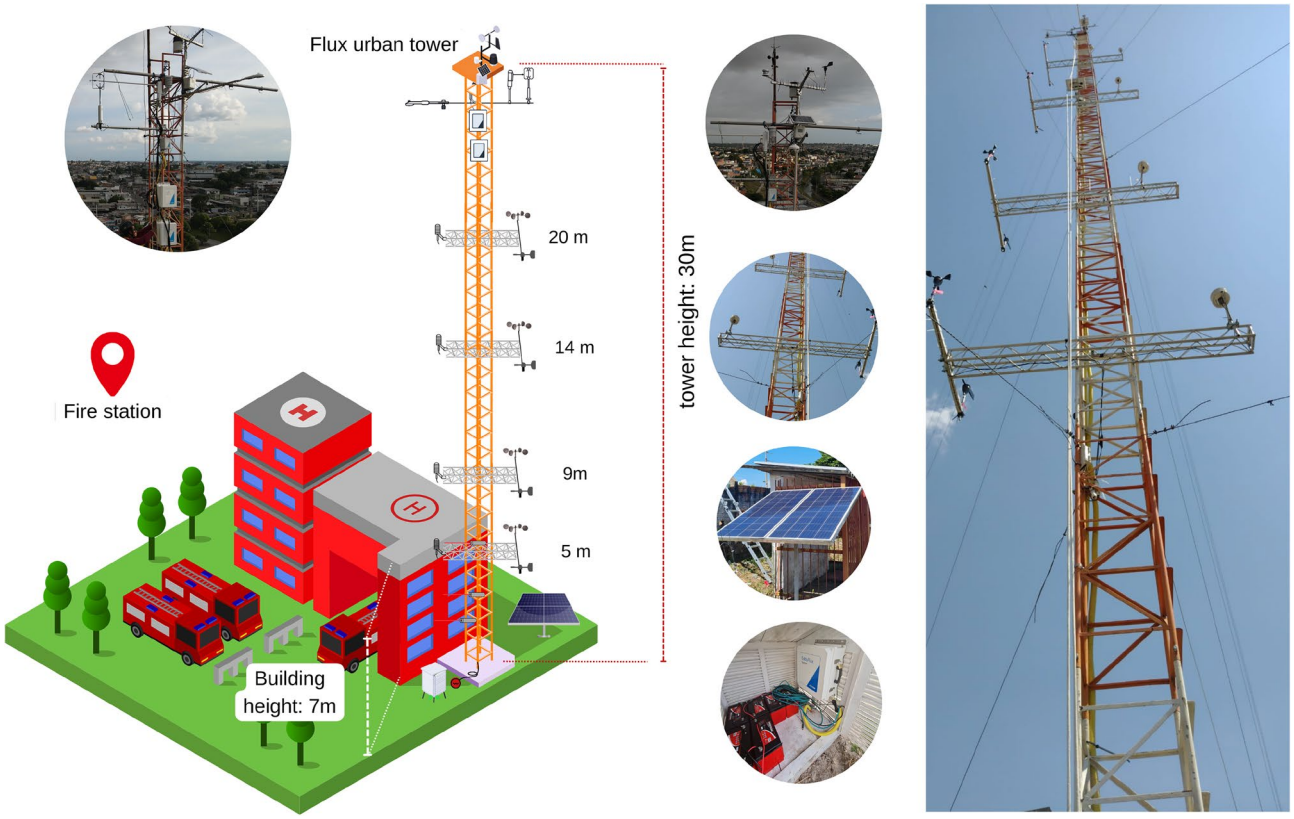

Fig. 2. Illustrative diagram of the Urban Micrometeorological Monitoring Tower in Manaus (TURB) and their arrangement at different measurement levels.

Instruments	Models	Height (m)	Variable	Sampling rate
3D Sonic Anemometer	WindMaster 3D, Gill Instruments Limited, UK	29.5	Three-dimensional wind speed and Sonic temperature	10 Hz
Closed-path H_2O and CO_2 Infrared Gas Analyzer	LI-7200 RS, LI-COR, Inc., USA	29.5	Carbon dioxide and water vapor	10 Hz
Net Radiometer	CNR4, Kipp & Zonen BV, Delft, Netherlands	30	Shortwave radiation and Longwave radiation	60 s
Heat Flux Plate	HFP01SC, Hukseflux Thermal Sensors BV, Delft, Netherlands	−0.5	Heat flux density	60 s
Thermohygrometer	S-THB-M002-Hobo, Onset Hobo	9, 14, 20, 30	Air temperature and relative humidity	60 s
Wind Speed Sensor	S-WSB-M003, Onset Hobo	9, 14, 20, 30	Wind speed and gusts	60 s
Wind Direction Sensor	S-WDA-M003, Onset Hobo	9, 14, 20, 30	Wind direction in degrees from true north	60 s
Rain Gauge	S-RGx-M002, Onset Hobo	30	Precipitation	Continuous
Infrared Radiometer	SI-111-SS, Apogee	1, 2, 5	Surface temperature	5 min

Table 1. Measurements conducted on the micrometeorological tower located in Manaus, AM, Brazil. Heights are referenced from ground level.

comprising a closed-path infrared gas analyzer for H_2O and CO_2 (LI-7200RS, LI-COR, Inc., USA) and a 3D sonic anemometer (WindMaster 3D, Gill Instruments Limited, UK), operating at a sampling frequency of 10 Hz. The soil heat flux plates were installed approximately 1 meter southeast of the tower base and buried horizontally at a depth of 5 cm in undisturbed soil, representative of the local urban surface, consisting of compacted clay and sparse grass cover.

Data processing

The estimates of turbulent fluxes were obtained from raw data following standard procedures for turbulent covariance calculation[12,52] using the EddyPro LiCor software version 7.0.8[53]. The software performs quality control on the 30-minute block averages[54,55]. These controls include: peak detection (spikes) and removal[56], coordinate rotation (double rotation)[57], and the Webb-Pearman-Leuning (WPL) density correction[58,59]. This

study used data collected during the wet and dry seasons of 2022, totaling 7, 048 30 minute runs. The wet season was defined as the quarter with the highest precipitation rates (February-March-April 2022), and the dry season as the quarter with the lowest precipitation rates (August-September-October 2022)[60].

The EddyPro outputs were subsequently filtered so that the fluxes were classified as good quality (flag 0), acceptable (flag 1), or poor quality (flag 2)[61]. Only data with flags 0 and 1 were included in the analysis, which means that runs with flag$= 2$ were excluded. After quality control, 959 ($\approx 13\%$) and 1, 192 ($\approx 17\%$) of the runs were rejected for *H* and *LE*, respectively.

Urban surface energy balance

From the first law of thermodynamics and the concept of control volume, the energy balance at an urban surface (SEB), assuming surface homogeneity and that there is no advection, SEB can be written[62]:

$$Rn + AH = H + LE + G + S \tag{1}$$

The left side of equation 1 represents the available energy. *Rn* is the net radiation ($Rn = SW_{in} - SW_{out} + LW_{in} - LW_{out}$), where SW and *LW* denote shortwave and longwave radiation fluxes, respectively, and the subscripts indicate whether the energy flux is incoming (in) or outgoing (out) from the surface. *AH* represents anthropogenic heat flux (from vehicular sources, stationary sources, and human metabolism). The terms *H* and *LE* are the vertical turbulent fluxes of sensible and latent heat, respectively, *S* is the heat stored in the urban canopy, and *G* is the ground heat flux. Although some studies have reported *AH* as negligible, others highlight its potential contribution based on factors such as latitude, energy demand, degree of industrialization and seasonal variability, as summarized by Shahmohamadi et al.[63]. However, it is important to note the challenge in directly measuring AH, as it is often incorporated into sensible heat flux, latent heat flux, stored heat, and longwave radiation flux[64]. Furthermore, its measurement is uncommon due to the complexity of the process and the need for advances in the development of new techniques. In the present study, *AH* was not considered, and its exclusion represents a limitation that should be addressed in future research.

Heat storage in the urban canopy (S)

In urban areas, *S* represents the absorption or release of energy/heat (per unit area and time) in the air layer within a volume (urban canopy), encompassing buildings/residences, vegetation, and soil. According to Michiles and Gielow[30], when there is a positive energy balance at the surface of the control volume - meaning that the incoming energy exceeds the outgoing energy - a convergent flux occurs ($S > 0$), resulting in surface warming. Conversely, when the outgoing energy exceeds the incoming energy, the surface cools due to a divergent flux ($S < 0$).

The *S* term can be estimated using the following indirect methods: energy balance residual, Thermal Mass Scheme (TSM), numerical simulation, and parameterization method[62]. The Thermal Mass Scheme (TSM) was chosen for this study due to its robustness in quantifying heat storage based on temperature variations in urban materials and their thermal properties. This method is based on the concept of air-soil-building volume at a local scale, proposed by Nunez and Oke[65], allowing for a more detailed and specific approach to complex urban systems. Additionally, as noted by Roberts et al.[66], the TSM offers the advantage of directly considering the thermal characteristics of the materials that make up the urban surface, providing greater accuracy in estimating the term S in the energy balance.

$$S = \sum_{i=1}^{n} S_i = \sum_{i=1}^{n} \frac{1}{A_i} \int C \frac{\Delta T}{\Delta t} \, dV_i \tag{2}$$

In Equation 2, the index *i* denotes the types of surface (e.g. roofs, walls), while *C* represents the thermal capacity of the material comprising the surface *i*. For this study, roofs were modeled as zinc sheets and walls as bricks and grout. The surface area (A_i) and the volume (dV_i) of each component were derived from urban surveys, assuming uniform material thicknesses (roofs: 0.15 m; walls: 0.2 m). Temperature changes ($\frac{\Delta T}{\Delta t}$) were obtained from infrared sensor measurements and combined with *C* to compute the contributions of heat storage (S_i). When integrated over the urban canopy layer (which may consist of multiple layers), equation 2 describes changes in heat storage resulting from the fluxes entering and exiting each built component within the system.

The sum of all components in the urban system gives the heat storage in the urban canopy. Here, we partitioned it into two main components: the roof (SHF_R) and the wall (SHF_W), so $S = SHF_R + SHF_W$. From equation 2, it is clear that estimating *S* requires temperature measurements of the surfaces comprising the investigated volume. In this study, we did not have these measurements available. To address this issue, infrared sensors were installed during an experimental campaign to monitor the surface temperature of the roof and wall of a building adjacent to the tower. The campaign took place from December 1 to 12, 2022, and involved the installation of four Apogee SI-111 IR infrared radiometer sensors (which measured surface temperatures from -55 to 55°C, (https://www.apogeeinstruments.com/si-111-ss-research-grade-standard-field-of-view-infrared-radiometer-sensor/). These sensors were strategically positioned: two directed at the wall, at heights of 2.5 and 1 m, respectively, and the other two installed at a height of 5 m, facing the roof.

Based on the infrared sensor temperature measurements during the intensive period, it was possible to correlate them with the thermohygrometer readings (data available for the entire analyzed year). For this purpose, a linear regression was performed between the air temperature measured by thermohygrometers at different levels (9, 14, 20, and 30 m) and the surface temperature of the roof and wall measured by the IR sensors (Fig. S1). Table 2 presents some of the statistical parameters obtained from the linear regression. It is noted that

		Statistical parameters			Linear regression coefficients		
y	$\hat{y}$	RMSE	MAE	R^2	Intercept	Slope	R^2
Roof	t9	3.22	1.98	0.52	−13.61	1.53	0.71
	t14	3.45	2.12	0.45	−13.44	1.54	0.67
	t20	3.24	2.02	0.52	−12.95	1.51	0.70
	t30	3.36	2.11	0.48	−13.80	1.55	0.69
Wall	t9	1.42	0.98	0.84	−8.92	1.34	0.94
	t14	1.67	1.14	0.78	−9.30	1.37	0.93
	t20	1.43	1.01	0.84	−8.57	1.33	0.94
	t30	1.60	1.12	0.79	−9.23	1.36	0.92

Table 2. Relationship between the surface temperature of walls and roofs and the air temperature at different levels (9, 14, 20, and 30 m), including the coefficients of the linear regression fit (y = observed values, $\hat{y}$ = modeled/predicted values).

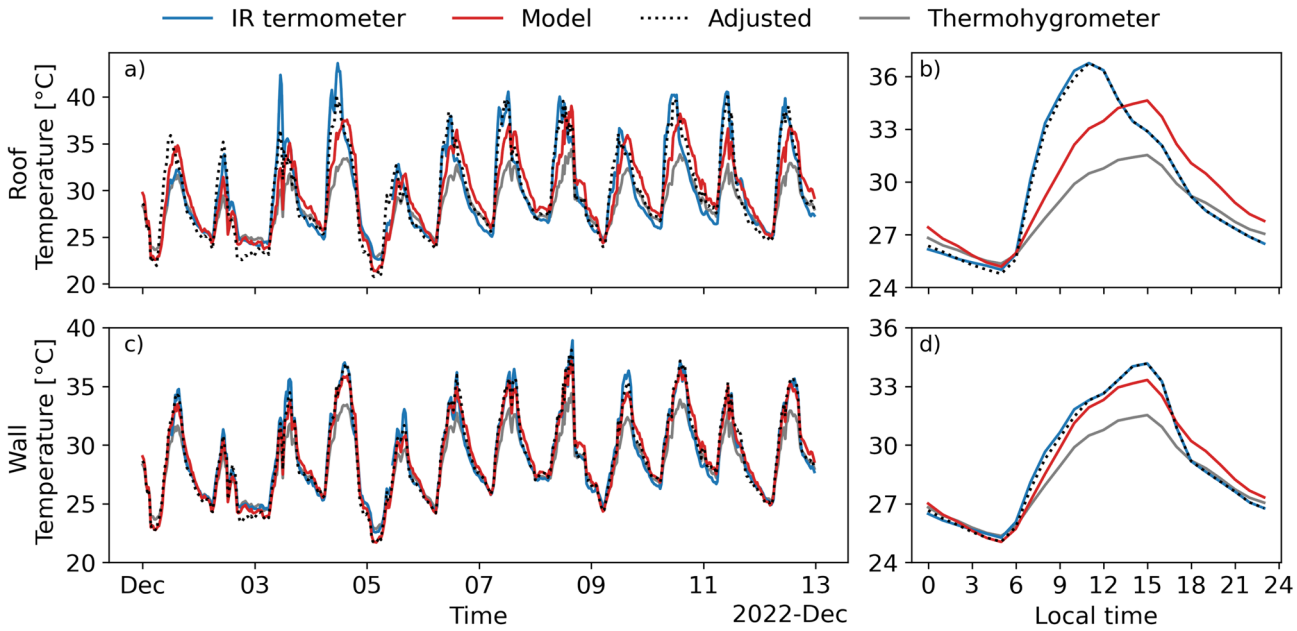

Fig. 3. Variability of the roof surface temperature (**a**) and wall surface temperature (**c**) and their respective mean diurnal cycles (**b** and **d**).

the best fit (R^2 : 0.71 for the roof and R^2 : 0.94 for the wall) occurred with the temperature recorded by the thermometer located at 9 m. Consequently, this measurement was used for the estimation of *S* for both wet and dry periods.

The correction of air temperature (obtained using the linear adjustment model shown in Table 2) still exhibited significantly underestimated values, particularly during the hottest hours of the day (Fig. S2 and Fig. 3b, d). The hourly mean error was used as a correction factor for the model estimates to address this issue. The hourly mean error is the difference between the temperature estimated by the model and the actual observed temperature at specific time intervals, as defined by the following equation.

$$T_{adjusted(i)} = T_{model(i)} - \overline{f_{(i)}} \tag{3}$$

where:

$T_{adjusted(i)}$: The corrected temperature at instant *i*.

$T_{model(i)}$: The temperature estimated by the model (Table 2) at time instant *i*.

$\overline{f_{(i)}}$: Correction factor, which is the value of the hourly mean error (model - observation) at time instant *i*, given by:

$$\overline{f_{(i)}} = \frac{1}{n}\left[\sum_{1}^{n}(T_{model(i)} - T_{observation(i)})\right] \quad (4)$$

where *n* is the number of days.

In Fig. 3, it can be observed that the temperature values measured at 9 m with the thermohygrometer and adjusted by equation 3 are very close to those observed with the IR sensors for the walls and roofs.

With the correction factor obtained by equation 3, the time series of the thermohygrometer temperatures at 9 m was adjusted. The TSM method is also based on the thermal storage capacity of the materials used to construct the wall and roof, considering the thermal capacity ($C = \rho.C_p$) of these materials. The values derived from the Brazilian Association of Technical Standards (ABNT NBR $15220 - 2 : 2005$) standards will be used for each material that composes the roof and wall surfaces, as shown in Table 3.

Energy balance closure

The surface energy imbalance (*IMB*) is considered the total contribution of neglected effects and uncertainties, which include at least one of the following terms: advection, natural and anthropogenic thermal processes, vertical flux divergences, and experimental uncertainty[67,68]. This study evaluated the balance closure using two methods adapted from Wilson et al.[69]. The first and primary method involved obtaining the linear regression coefficients (slope, intercept, and coefficient of determination - R^2) of the ordinary least squares (OLS) relationship between the half-hourly estimates of net radiation (*RN*) and the sum of the non-radiative flux densities ($H + LE + G + S$) during each season. The ideal closure is represented by the values 0, 1, and 1 for the intercept (b), slope (a), and determination coefficient (R^2), respectively.

$$IMB = Rn - (H + LE + G + S) \quad (5)$$

$$H + LE + G + S = aRn + b \quad (6)$$

The second method used was the Energy Imbalance Factor (EIF), which indicates the magnitude of the energy balance non-closure. To obtain the EIF, it is first necessary to calculate the Energy Balance Ratio (EBR), given by the ratio of the cumulative sum of $H + LE + S + G$ to *Rn* during the investigated period.

$$EBR = \frac{\sum(H + LE + G + S)}{\sum(Rn)} \quad (7)$$

$$EIF = EBR - 1 \quad (8)$$

Results and discussion

Meteorological conditions during the study period

Figure 4 presents the monthly mean air temperature and cumulative precipitation recorded at the urban experimental site (TURB), along with the climatological normals for the period $1991 - 2020$ from the INMET (National Institute of Meteorology) database. Temperature values were measured at $9\,m$ (the lowest level) above the ground at TURB. The period from January to April is notable for its higher monthly precipitation totals, with a maximum value recorded in April ($328.6\,mm$). Additionally, the precipitation values measured at TURB were quite similar to the climatological average. In contrast, June, July, and August showed significantly lower precipitation than the climatological average expected for this period. This substantial reduction in precipitation indicates an intense and atypical dry period.

During the wet season (months from January to April), temperatures were close to the climatological average (around $26\,^{\circ}\mathrm{C}$). This behavior suggests that during this period, climatic conditions were relatively stable, with temperatures remaining within a range near the expected average value. However, a gradual increase in temperatures was observed beginning in May, surpassing the climatological average between July and September. This period was characterized by higher temperatures than expected for the region, indicating a phase of intense warming. September was the hottest month, with maximum temperatures around $30\,^{\circ}\mathrm{C}$.

In Fig. 5a, it can be observed that during the wet season, the predominant wind direction is NE (11.4%) and E (9.2%) with wind speeds ranging from 1 to $4.9\,\mathrm{ms}^{-1}$, and to a lesser extent from the N. In the dry season (Fig. 5b), the NE and SE prevail, both in terms of magnitude (with speeds ranging from 1 to $5.7\,\mathrm{ms}^{-1}$) and frequency ($> 8\%$). Stronger winds ($> 4.1\,\mathrm{ms}^{-1}$) of S and SW are also observed.

			Wall		Roof
	Units	Air	Brick[1]	Grout[1]	Zinc[1]
ρ	$\mathrm{kg\,m^{-3}}$	1.225	1600	2000	7100
C_p	$\mathrm{J\,kg^{-1}\,K^{-1}}$	1004	920	1000	380
C	$\mathrm{Jm^{-3}\,K^{-1}}$	$1.23E+03$	$1.47E+06$	$2.00E+06$	$2.70E+06$

Table 3. Physical properties of the construction materials that make up the wall and roof. [1] ABNT NBR 15220-2:2005

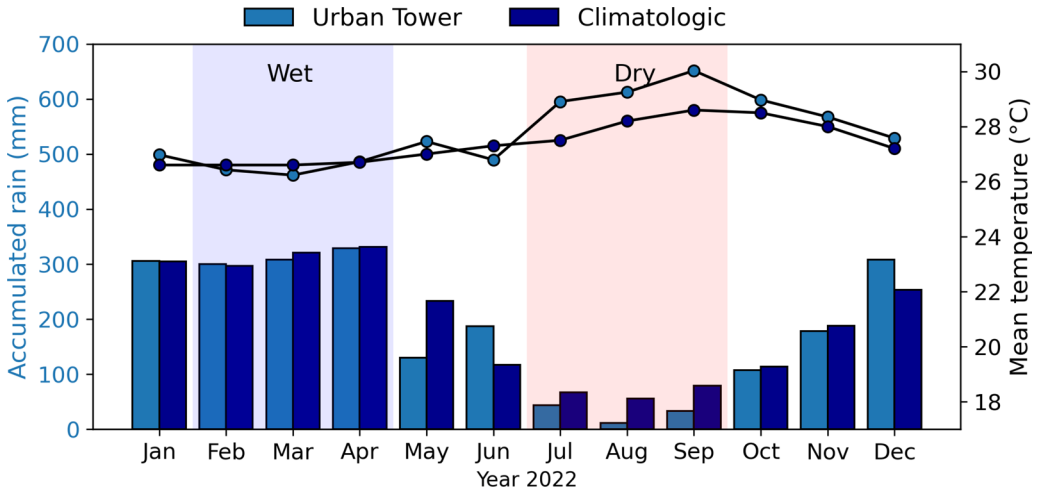

Fig. 4. Monthly values of accumulated precipitation (bars) and average air temperature (lines) for the TURB station during 2022 (light blue) and climatological normals (dark blue) for Manaus (1991 to 2020), based on data from the National Institute of Meteorology (INMET).

To analyze the contribution of different areas surrounding TURB to the turbulent fluxes, a footprint estimation was conducted, according to Kljun et al.[70]. The probability density function, which describes the upwind distance for the 90% flux contribution, reveals notable differences based on wind direction between the wet and dry seasons (Fig. 5c and d). During the wet season, the distance is greater in the E and NE directions, ranging from 400 to 430 m. In the dry season, the mean distance for 90% contribution in the predominant wind direction is approximately 500 m, with significant contributions from the NE, E, and SE.

Therefore, during the wet season, the primary source area for turbulent fluxes is observed in the predominant wind direction from the NE-E sector, where there is a strong presence of impermeable surfaces such as streets and residences, and secondarily in the N-NE direction, influenced by urban infrastructure, including paved areas (Fig. 1c). In the dry season, the primary source area for turbulent fluxes remains in the NE-E direction. However, the secondary source area for turbulent fluxes shifts to the SE-S sectors, where green areas contribute more significantly (Fig. 1c).

Radiation fluxes

Figure 6 shows the values of shortwave (incident and reflected) and longwave radiation components (incident and emitted), and net radiation (*Rn*) for the wet and dry seasons in the TURB. It is evident that during the wet season (Fig. 6a), the magnitudes of SW_{in} are substantially lower compared to the dry season (Fig. 6b). This is particularly noticeable between 10:00 LT and 14:00 LT, where SW_{in} during the dry season ($\approx 780\,\mathrm{Wm^{-2}}$ at 11:00 LT) exceeds the corresponding values during the wet season ($\approx 530\,\mathrm{Wm^{-2}}$ at 12:00 LT), with a maximum difference of $267\,\mathrm{Wm^{-2}}$ at 11:00 LT. Furthermore, the SW_{in} values during the wet season exhibited greater variability (shaded area) compared to the dry season, which can be attributed to the higher cloud cover during this period, consistent with the well-documented seasonal atmospheric dynamics of the central Amazon region[71]. These results shows similarities with the SW_{in} values reported by Malhi et al.[27], who used data measured at the Rio Cuieiras experimental site (also named ZF2), located north in a forested area 60 km from Manaus. Their study demonstrated a difference of $166\,\mathrm{Wm^{-2}}$ between the SW_{in} values during the dry and wet seasons (from $730\,\mathrm{Wm^{-2}}$ in the dry season to $564\,\mathrm{Wm^{-2}}$ in the wet season at 13:00 LT, as shown in their Fig. 3). Roth et al.[18] showed that in a tropical city like Singapore, the variation in SW_{in} was $629\,\mathrm{Wm^{-2}}$ (wet season) and $715\,\mathrm{Wm^{-2}}$ (dry season), with these values being relatively close to those found in this work. Manaus and Singapore are both cities located in the tropical region, where the presence or absence of clouds during the wet and dry seasons plays a crucial role in SW_{in} values.

Conversely, for a megacity like São Paulo, the difference in SW_{in} values measured during the wettest and driest months was only $36\,\mathrm{Wm^{-2}}$ (Ferreira et al.[72]; their Table 7), indicating a less pronounced seasonal variation compared to that observed in Manaus. São Paulo does not experience as high cloud cover compared to these two cities, and therefore the variation in SW_{in} between summer and winter is smaller[18,29,72].

The SW_{out} values (Fig. 6d, e) show seasonal variability similar to that of SW_{in} in terms of variation, amplitude, and anomalies, with the highest (lowest) values observed during the dry (wet) season. During the wet season, the maximum value was $82\,\mathrm{Wm^{-2}}$ at 12:00 LT, and during the dry season, it was $135\,\mathrm{Wm^{-2}}$ at 11:00 LT.

In Fig. 6g and h, the hourly values of incoming longwave radiation (LW_{in}) are shown. It is noted that LW_{in} exhibited similar maximum values during both wet and dry seasons ($\approx 442\,\mathrm{Wm^{-2}}$). During the dry season, a gradual and prolonged decline in LW_{in} was observed after the maximum, resulting in a minimum of $410\,\mathrm{Wm^{-2}}$ at 06:00 LT. In contrast, during the wet season, the minimum value of LW_{in} was approximately $421\,\mathrm{Wm^{-2}}$ at 04:00 LT. Therefore, during the wet season in the Amazon, LW_{in} values tend to be higher compared to the dry season[29]. The LW_{in} values reported by von Randow et al.[29] over the Amazon rainforest ranged from approximately 400 to $440\,\mathrm{Wm^{-2}}$ during the wet season and 390 to $440\,\mathrm{Wm^{-2}}$ during the dry

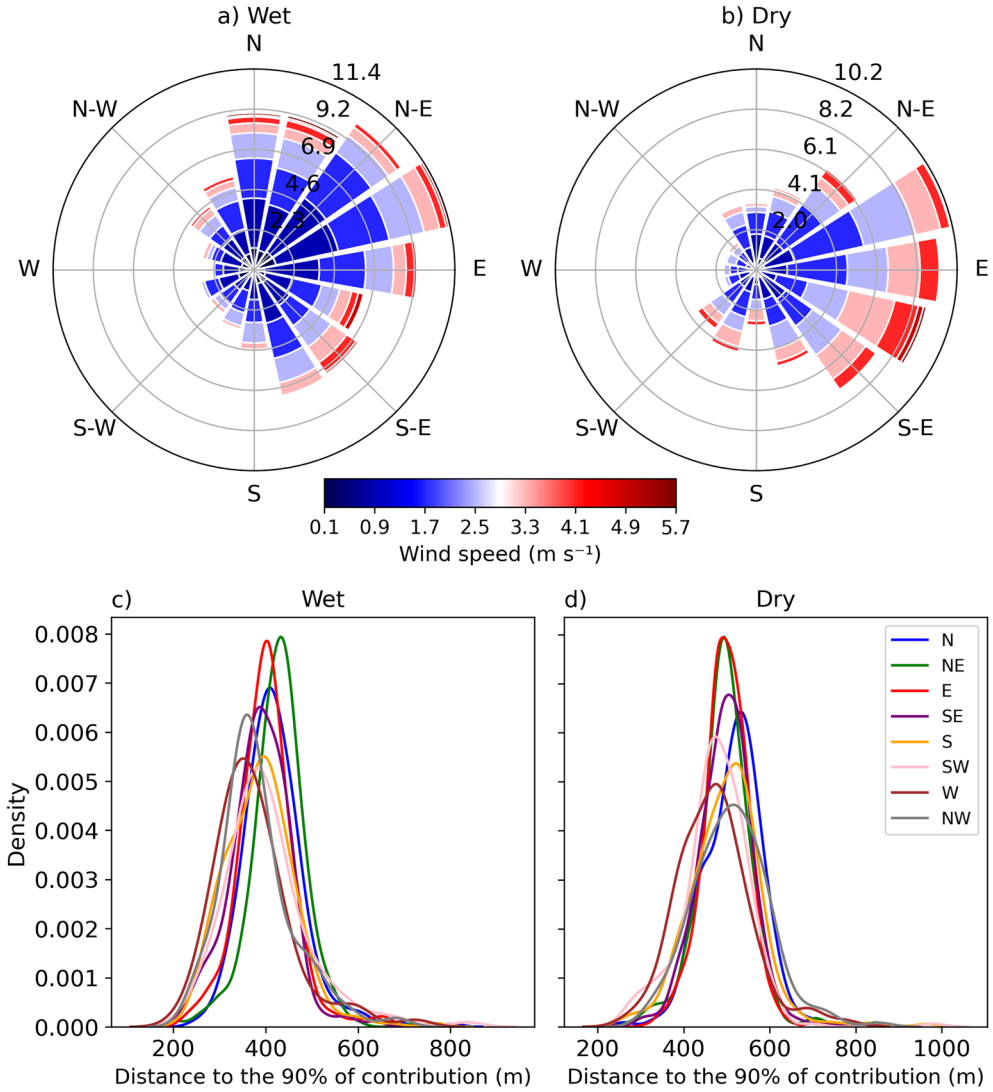

Fig. 5. (**a**, **b**) Wind rose for the wet and dry seasons. The colors represent the average wind speed. (**c**, **d**) Probability density function of the distance of the 90% flux contribution based on wind direction for the wet and dry seasons.

season. For a tropical city like Singapore, LW_{in} values ranged from 413 to 445 Wm^{-2} and 390 to 430 Wm^{-2} during the wet and dry seasons, respectively[18]. In a subtropical city like São Paulo, Brazil, values ranged from 377 Wm^{-2} to 436 Wm^{-2} for the summer (February) and from $329-388$ Wm^{-2} for the winter (August)[72]. It is observed that the LW_{in} values for Manaus are not significantly different from those observed over other sites at Amazon rainforest or in tropical regions like Singapore.

The LW_{out} values (Figs. 6j,k) were considerably lower during the wet season (ranging from 445 to 484 Wm^{-2}) compared to the dry season (ranging from 451 to 527 Wm^{-2}). This result was expected since the warmer surface during the dry season will emit a higher longwave radiation flux. The maximum difference in LW_{out} values between the seasons was 40 Wm^{-2}, occurring between 11:00 LT and 13:00 LT (Fig. 6l). The LW_{out} (max) values found for the Amazon rainforest, Singapore, and São Paulo were: $426-475$ Wm^{-2} (wet) and $428-475$ Wm^{-2} (dry), $444-499$ Wm^{-2} (wet) and $455-511$ Wm^{-2} (dry), and $400-497$ Wm^{-2} (August) and $455-511$ Wm^{-2} (February), respectively[18,29,72]. It is noted that the LW_{out} values for the city of Manaus were much closer to those of Singapore and São Paulo than to those observed over the Amazon rainforest, especially during the dry season. This indicates that the heat absorption dynamics in the urban canopy differs from those observed in the forest canopy. In the urban landscape, the three-dimensional geometry allows for multiple reflections of incident radiation, leading to a significant increase in the capture and absorption of energy by the surface. Additionally, heat conduction and convection processes play a crucial role, significantly contributing to higher longwave radiation emission from the urban surface.

The maximum net radiation (*Rn*) values in Manaus were 410 and 565 Wm^{-2} during the wet and dry seasons, respectively (Figs. 6i-j). The lower *Rn* values during the wet season are often attributed to the higher cloud cover, which reduces SW_{in} in this period. However, when comparing the *Rn* values found here with those measured

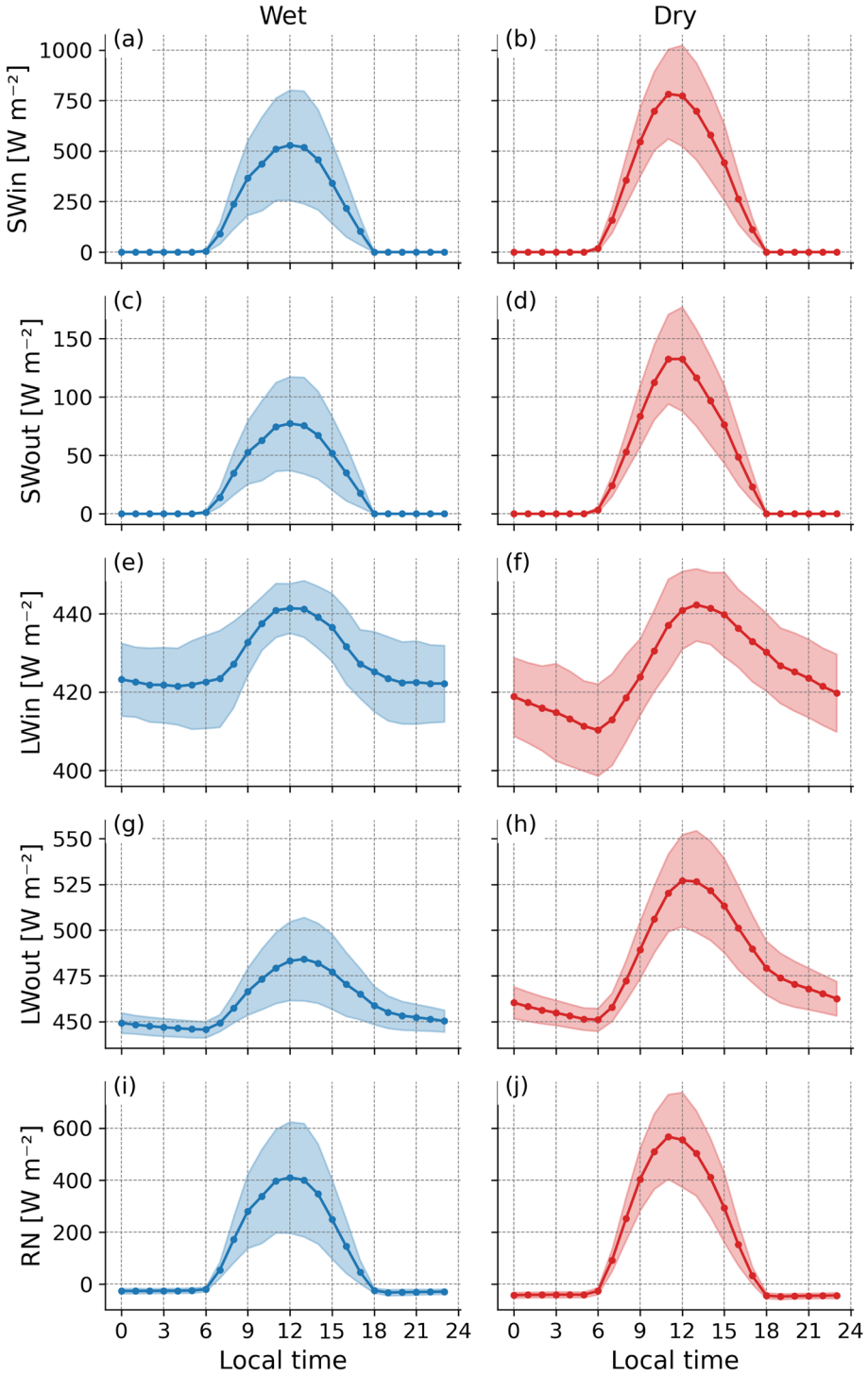

Fig. 6. Daily variability of the radiation balance components during the wet season (blue) and dry season (red). SW_{in} and SW_{out} represent the components of incoming (**a**, **b**) and reflected (**c**, **d**) shortwave radiation, respectively. The components of longwave radiation emitted by the atmosphere and surface are represented by LW_{in} (**e**, **f**) and LW_{out} (**g**, **h**). And (**i**, **j**) net radiation ($RN = SW_{in} - SW_{out} + LW_{in} - LW_{out}$).

above the Amazon rainforest (556 Wm^{-2} in the wet and 623 Wm^{-2} in the dry season), Singapore (473 Wm^{-2} in the wet and 527 Wm^{-2} in the dry season), and São Paulo (452 Wm^{-2} in August and 520 Wm^{-2} in February), we observe that the values for Manaus were considerably lower than those measured over the Amazon rainforest. This discrepancy is likely due to the relatively higher LW_{out} values in urban areas compared to forested regions.

The average albedo values (Fig. 7), which represent the ratio of SW_{out} to SW_{in}, ranged from 0.15 to 0.18 for the wet and dry seasons, respectively. There are no previous reports on the seasonal variation of surface albedo

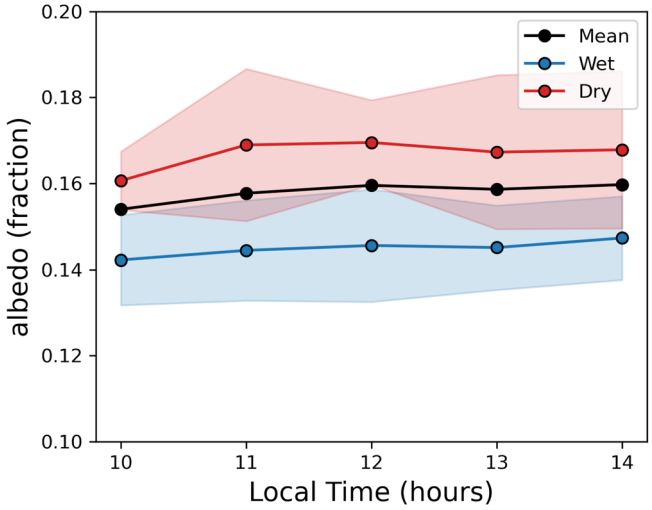

Fig. 7. Diurnal variability (10:00 LT to 14:00 LT) of the albedo for the overall mean (black), wet season (blue), and dry season (red), measured at the urban tower in the city of Manaus.

in urban areas of the Amazon. The albedo values found for the metropolitan region of Manaus were higher than those (0.13) measured over the Amazon rainforest[29]. The values observed here are consistent with typical values reported in the literature for urban and suburban areas in other regions located at mid-latitudes (mean albedos of 0.14 and 0.15, respectively)[73]. These values also resemble those observed under seasonal conditions in a tropical city like Singapore, which were approximately 0.15 and 0.17 for wet and dry conditions, respectively[18].

Based on the results of the Student's t-test (t-statistic of -24.34 and p-value = 0), we can conclude that the albedo during the wet season was significantly different from the albedo during the dry season. The negative t-statistic suggests that the mean albedo during the wet season is significantly lower than the mean albedo during the dry season. Furthermore, the p-value being approximately zero indicates that the probability of observing such a large or greater difference in albedo between the two seasons, under the assumption that there is no real difference, is virtually nil. Therefore, surface reflectivity varies significantly between the wet and dry seasons.

Components of energy balance

The components of the energy balance, such as the turbulent fluxes of sensible heat (H) and latent heat (LE), as well as soil heat flux (G), for both the wet and dry seasons, are shown in Fig. 8. H values remained positive during both day and night (Figs. 8a–b), with higher values observed during the dry season, reaching a maximum of $251\ \mathrm{Wm}^{-2}$, compared to $119\ \mathrm{Wm}^{-2}$ in the wet season, both occurring at 12:00 LT. The minimum values were recorded at 06:00 LT during the wet season $(0.53\ \mathrm{Wm}^{-2})$ and at 05:00 LT during the dry season $(3.60\ \mathrm{Wm}^{-2})$. The differences were more significant during the daytime (Fig. 8c), where H was at least 100% higher $(>100\ \mathrm{Wm}^{-2})$ during the dry season between 10:00 LT and 13:00 LT.

Sensible heat flux remained positive even after Rn had changed sign during the night, exhibiting a distinct dynamic compared to forested regions. In urban areas like Singapore[18], H stays positive after sunset, becoming slightly negative between 05:00 LT and 06:00 LT. According to Oke et al.[62], there is a direct relationship between the magnitude of nocturnal positive H and urban built density. This relationship is evident in high-density cities such as Tokyo, Japan; Basel, Switzerland; Marseille, France; and Mexico City, Mexico, which are characterized by local climate zones (LCZ) classified as "compact midrise" and "lowrise" (LCZ 2 and LCZ 3). In these cities, nocturnal H remains positive, with average values ranging between $5\ \mathrm{Wm}^{-2}$ and $30\ \mathrm{Wm}^{-2}$ from 21:00 LT to 03:00 LT[62]. Conversely, in suburban area from São Paulo, H is relatively small at night, becoming negative approximately one hour after Rn turns negative and remaining so until sunrise[17].

In the Amazon rainforest, H values are negative during the night[27,29]. However, during the day, the H values observed in Manaus were similar to those recorded in the Jaru Biological Reserve (Rebio-Jaru), located in the southwestern Amazon, with maximum values of $117\ \mathrm{Wm}^{-2}$[29]. During the dry season, H values in Manaus reached a maximum of $250\ \mathrm{Wm}^{-2}$, exceeding those reported for Rebio-Jaru (maximum of $180\ \mathrm{Wm}^{-2}$)[29] and approaching values observed in Singapore $(226\ \mathrm{Wm}^{-2})$[18].

The behavior of LE (Figs. 8d, e) was similar in both seasons, with a decline after reaching its peak: $132\ \mathrm{Wm}^{-2}$ at 12:00 LT during the wet season and $121\ \mathrm{Wm}^{-2}$ at 11:00 LT during the dry season. Between 12:00 and 17:00 LT, LE values were higher in the wet season, with a maximum difference of approximately $20\ \mathrm{Wm}^{-2}$ (Figure 8f). In contrast, during the other hours of the day, LE values were higher in the dry season, although the difference did not exceed $10\ \mathrm{Wm}^{-2}$. Despite seasonal variations and the decrease in rainfall volume and frequency during the dry season, LE in Manaus does not appear to be significantly affected by this reduction in rainfall. This indicates that other factors and processes may play a role in influencing LE values in the urban area of Manaus.

The LE values reported by von Randow et al.[29] for the Amazon rainforest (Rebio-Jaru) were higher than those observed in Manaus, with maximum values reaching approximately $400\ \mathrm{Wm}^{-2}$. This outcome aligns with the well-documented high evapotranspiration rates of the Amazon rainforest throughout the year, attributed to its

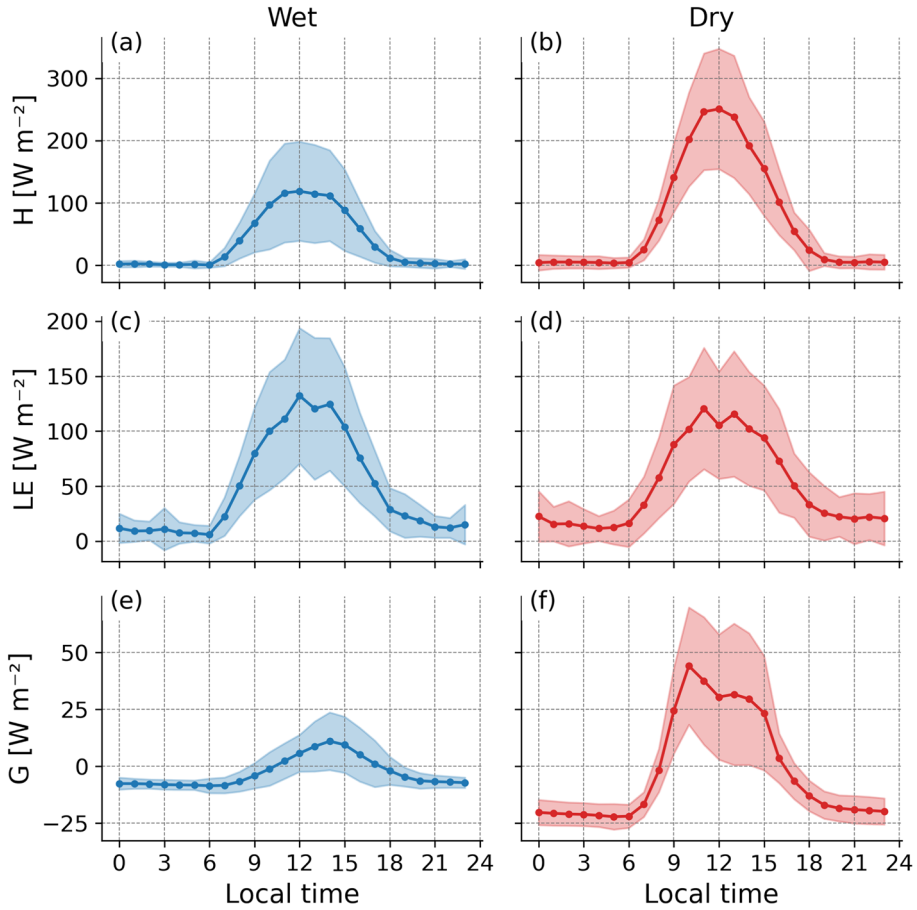

Fig. 8. Mean diurnal variation of the components of turbulent sensible heat flux - *H* (**a**, **b**), latent heat flux - *LE* (**c**, **d**), and soil heat flux (**e**, **f**) during the wet season (blue) and dry season (red). The shaded areas correspond to the statistical error of the mean.

soil's greater water storage capacity. Nonetheless, a shared characteristic between Manaus and Rebio-Jarú is the weak seasonality in *LE* values.

In the case of Rebio-Jarú, von Randow et al.[29] showed that the deep roots of trees could access water at greater depths during the dry season, maintaining their evapotranspiration rates, and thus, *LE* values did not show significant decreases from the dry to the wet season. In urban Manaus, it is observed that during the dry season, there is runoff coming from the SE-S-SW direction (Fig. 5), where there is greater green cover (Fig. 1c), which may explain the *LE* values during the dry season being similar to those observed during the wet season. Additionally, we believe that the low variability of *LE* between the wet and dry seasons in Manaus is related to the presence of moisture sources (large rivers), which contribute to maintaining high *LE* values during the dry season.

In a tropical city like Singapore, the seasonal variability of *LE* was also low, varying within a narrow range during the wet and dry seasons, with values of $123\,\mathrm{Wm}^{-2}$ and $105\,\mathrm{Wm}^{-2}$, respectively[18]. In a subtropical city like São Paulo, *LE* showed seasonal variations, with values of $< 50\,\mathrm{Wm}^{-2}$ during the dry season and approximately $112\,\mathrm{Wm}^{-2}$ during the wet season[74].

G represents the variation in heat storage and release in the soil. The soil accumulates energy during the day (positive) and releases it (negative) at night, after sunset. During the wet season, *G* reached $11\,\mathrm{Wm}^{-2}$ at 14:00 LT, while in the dry season, it reached $44\,\mathrm{Wm}^{-2}$ around 10:00 LT, which is four times higher. The most pronounced hourly differences occurred between 09:00 LT and 13:00 LT, exceeding $20\,\mathrm{Wm}^{-2}$. At night (20:00 LT to 05:00 LT), the dry season released ($G < 0$) on average $13\,\mathrm{Wm}^{-2}$ more heat than the wet season (dry: $-20.20\,\mathrm{Wm}^{-2}$ vs. wet: $-7.32\,\mathrm{Wm}^{-2}$). However, near sunrise and sunset, the differences between seasons became less significant, despite the wet season generally recording higher values. The increase in *G* during the dry season is due to lower cloud cover and, consequently, higher incident solar radiation on the surface, causing the soil to absorb and release more heat into the atmosphere.

In the forest, soil heat flux is generally low and does not show significant seasonal variation[30], mainly due to the limitation of solar radiation caused by the dense forest canopy. Therefore, it is added to the heat storage term in biomass and air above the forest floor[75]. On the other hand, in pasture areas, heat flux is higher than in the forest and exhibits notable seasonal variations[29], similar to those observed in this study.

Storage heat flux

The values of SHF_W (Fig. 9 a and b) and SHF_R (Fig. 9 c and d) showed similar variability during both dry and wet periods, although SHF_R was slightly lower. Both variables peaked around 8:00 LT, earlier than the typical peak time of sensible heat flux and latent heat flux. These earlier peaks are due to the low thermal capacity of the materials composing the roof and walls. The maximum SHF_W value was approximately 25 Wm^{-2} higher during the dry season than the wet season, while the maximum SHF_R value remained nearly unchanged between the seasons.

SHF_R values became negative around 14:00 LT in both seasons, while SHF_W became negative at 16:00 LT. An explanation for this time lag in the behavior of SHF_R and SHF_W is the average heat storage/release capacity of each surface type (roof and wall) in the urban system. Large temperature gradients produce sudden changes in the rate of heat absorption and release, such as the "peak" in energy absorption during the early morning and the abrupt drop toward energy release (negative) in the early evening[66]. Heat release occurs faster from the roof than from the wall due to zinc's lower thermal capacity (Table 3). Total heat storage in the urban layer (Figs. 9e, f) is predominantly influenced by the behavior of SHF_W, contributing an average of 72% daily during the wet season and 97% during the dry season. The maximum S value was 102 Wm^{-2} (wet season) and 127 Wm^{-2} (dry season) at 08:00 LT, with a minimum at 18:00 LT (approximately -81 Wm^{-2} in the wet season and -102 Wm^{-2} in the dry season). During the wet season, the urban canopy had greater average heat accumulation, reaching approximately 4.26 Wm^{-2}, due to lower dissipation (minimum value). In contrast, heat absorption and release were higher during the dry season, leading to a smaller energy storage of 2.17 Wm^{-2}.

In forest environments, heat storage is primarily partitioned between biomass and the air above the ground[75]. The variability of S in the urban environment was similar to that observed in forests during the dry season[30] but higher in magnitude (max: 64 Wm^{-2}, min: -32 Wm^{-2}), due to the different thermal properties of urban and forested surfaces. Additionally, in forests, heat storage in tree trunks accounts for about 40% of the total energy storage[30]. On the other hand, the maximum storage (242 Wm^{-2}) and maximum release (-98 Wm^{-2}) reported by Ferreira et al.[17] were higher than the values found in this study.

Surface energy balance

The seasonal variation of the energy balance, including all convective and conductive flux components, is showed in Fig. 10. During the wet season, the H and LE exhibit similar behavior. LE plays a dominant role in

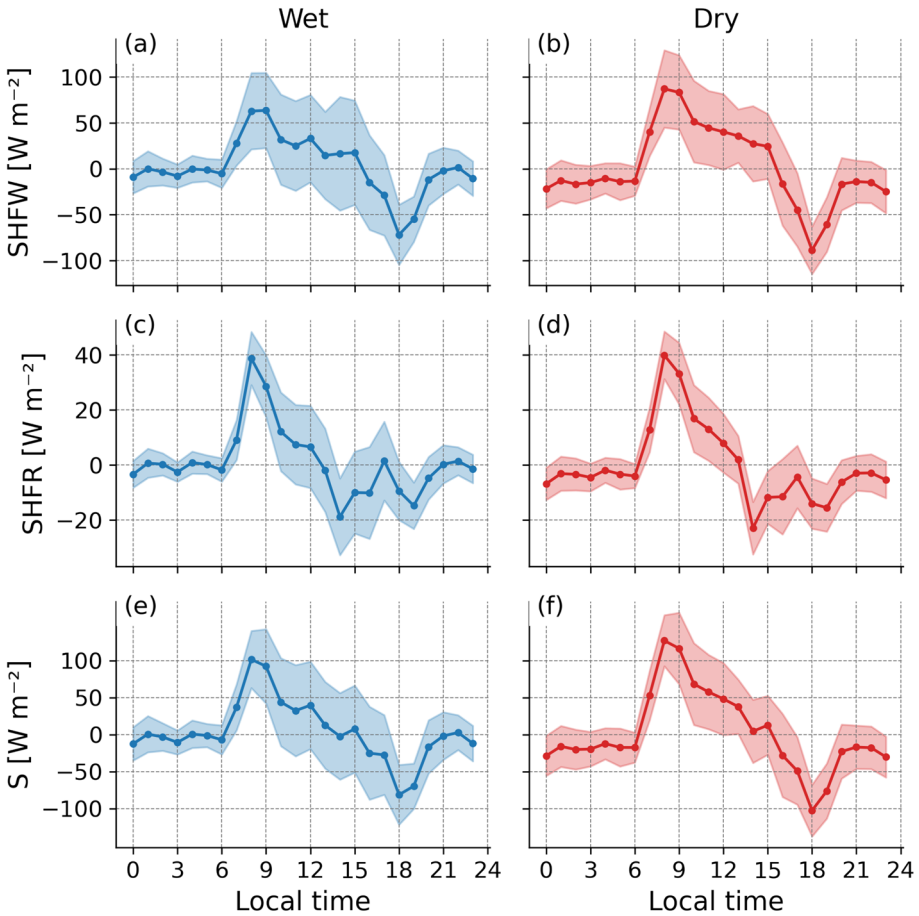

Fig. 9. Mean daily variation of the stored heat flux in the wall - SHF_W (**a**, **b**), roof - SHF_R (**c**, **d**), and the total sum - S (**e**, **f**) for the dry (red) and wet (blue) seasons.

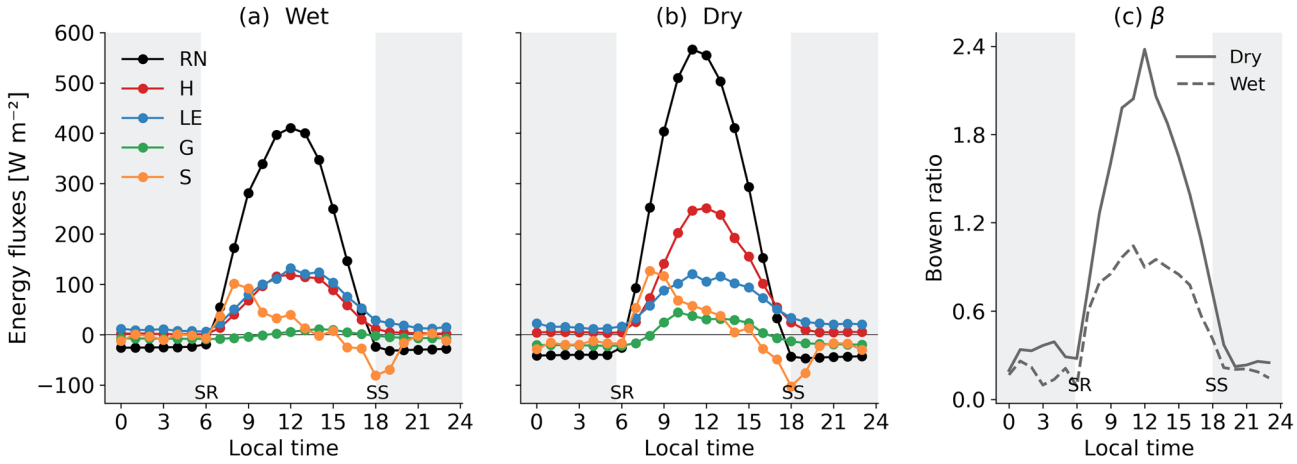

Fig. 10. Daily variability of the hourly mean values of observed components (*H*, *LE*, and *G*) and estimated (*S*) during the wet (**a**) and dry (**b**) seasons; and Bowen ratio (**c**). SR – sunrise, SS – sunset.

energy partitioning, accounting for approximately 46% of the daily energy, while *H* represents 36%, and *G* and heat stored in the canopy *S* contribute 3% and 4%, respectively.

This pattern differs from observations in other urban regions, including tropical areas such as Singapore[18], where a distinct scenario was observed. In Singapore, during the wettest period, *H* was 22% higher than *LE* and accounted for around 52% of *Rn*. However, in a suburban area of São Paulo, during the summer/wet season, the values were similar to those observed here for the wet season (*LE* was 14% higher than *H*, while *H* accounted for around 32% and *LE* about 36% of *Rn*). This observation is related to the presence of vegetation, soil moisture content, and circulation patterns influenced by sea breezes that transport moisture inland[74].

Sensible heat flux dominates energy partitioning during the dry season, contributing about 55% of the total, with an average daily value of $6.36\,\mathrm{MJm^{-2}d^{-1}}$. The remaining fluxes contribute 37% (*LE*: $4.30\,\mathrm{MJm^{-2}d^{-1}}$) and 2% (S:$0.19\,\mathrm{MJm^{-2}d^{-1}}$ and G: $-0.20\,\mathrm{MJm^{-2}d^{-1}}$) to the daily average. Overall, the energy balance resembles that measured in other urban areas across various latitudes and climatic conditions. Most of the available energy at the surface during the day is transferred to the urban canopy through turbulent convection (i.e., *H*), evaporation from surfaces (*LE*: $7.40\,\mathrm{MJm^{-2}d^{-1}}$), and a smaller fraction through conduction ($G + S$: $5.1\,\mathrm{MJm^{-2}d^{-1}}$). Thus, during this period, there is a greater accumulation of energy due to the seasonal conditions, with this energy primarily directed towards surface heating.

The *H* and *LE* observed in this study exceeded those reported in Singapore (tropical city)[18] during a comparable dry season, as well as those measured in São Paulo, a large metropolitan area in southeastern Brazil[17]. Notably, both *H* and *LE* were also higher than the values obtained during one the first eddy covariance observations of energy fluxes in the Amazon, conducted at the Ducke Reserve in 1983[21] (approximately 25 km from Manaus in 1983 but now encompassed by the city). Shuttleworth et al.[21] reported that *LE* accounted for approximately 70% of net radiation during the dry season (LE = $8.42\,\mathrm{MJm^{-2}d^{-1}}$; $Rn = 12.06\,\mathrm{MJm^{-2}d^{-1}}$). In contrast, in our urban study site, *LE* represented only 37% of *Rn* ($LE = 4.30\,\mathrm{MJm^{-2}d^{-1}}$; $Rn = 11.66\,\mathrm{MJm^{-2}d^{-1}}$). This substantial reduction in the proportion of energy allocated to *LE* was accompanied by a corresponding increase in *H*, which increased from $2.85\,\mathrm{MJm^{-2}d^{-1}}$ (24%) in the Ducke Reserve[21] to $6.36\,\mathrm{MJm^{-2}d^{-1}}$ (55%) in our measurements. These changes are particularly relevant considering that the Ducke Reserve, once a site of primary forest, has become increasingly surrounded by Manaus'urban development[76]. It highlights how urbanization alters surface energy partitioning, with potential implications for urban climate.

Urban heat storage plays a significant role in energy distribution during sunrise and sunset. Together with soil heat flux, it significantly influences the heating of the urban canopy, particularly during the wet season, where *S* is 48% and *G* is 17% higher than in the dry season. During the nighttime, these contributions account for 74% and 48% of the available energy, respectively (Table 4).

The diurnal and nocturnal trends for the convective and conductive fluxes are reflected in the corresponding daily averages (Table 4). The seasonal variability of *Rn* and *H* during the daytime was similar to the daily pattern, with higher values during the dry season. In contrast, *LE*, *G*, and *S* showed an opposite pattern, with higher values during the wet season. However, only the nighttime seasonal behavior mirrored the daily average.

The maximum Bowen ratio (β) during the day was observed near midday (Fig. 10c). The highest daytime values (≈ 2.37) were recorded during the dry season, when *H* was significantly higher than during the wet season (≈ 1.05). Values higher than 1 indicate that the surface directs more heat as *H* and are typical of dry surfaces, while values smaller than 1 indicate that *LE* dominates, which is characteristic of moist surfaces. The daytime results were lower than those found for Singapore (β values of 1.31 and 1.96 during the dry and wet seasons, respectively)[18]. The daily average of the Bowen ratio during the wet season (0.88) was comparable to that of São Paulo, but was lower during the dry season (1.98)[74].

	Averaged energy flux ($MJm^{-2}d^{-1}$)					
	Daily value (24h)		Day value (Rn> 0)		Night value (Rn< 0)	
	Wet	Dry	Wet	Dry	Wet	Dry
RN	9.01	11.66	22.35	29.64	−3.56	−2.29
H	3.22	6.36	6.73	13.19	0.58	0.25
LE	4.12	4.30	7.64	7.40	1.68	1.15
G	−0.24	−0.20	0.18	1.57	−1.70	−0.60
S	0.37	0.19	2.46	3.53	−2.64	−1.40
Components ratio						
γH	0.36	0.55	0.30	0.45	0.16	0.11
γLE	0.46	0.37	0.34	0.25	0.47	0.50
γS	0.04	0.02	0.11	0.12	0.74	0.61
γG	0.03	0.02	0.01	0.05	0.48	0.26
ε	0.56	0.40	0.53	0.36	0.74	0.82
β	0.78	1.48	0.88	1.78	0.34	0.22

Table 4. Summary of energy fluxes ($MJm^{-2}d^{-1}$). Average hourly value estimates for the wet and dry season. Diurnal values are integrated when $Rn > 0$. Daily values are integrated over 24 hours. γ = components ratio (energy fluxes/Rn) ε = evaporative fraction $LE/(LE + H)\beta$ = Bowen ratio (*H*/*LE*)

Energy balance closure

The linear regression coefficients between the sum of energy fluxes and the energy balance, using Ordinary Least Squares (OLS) for all half-hour data in both the dry and rainy seasons, are presented in Fig. 11. The energy fluxes, $H + LE$ (and the inclusion of the conductive terms, *S* and *G*) versus *Rn* exhibited relatively high values in both seasons, with a correlation coefficient (R^2) varying from 0.78 to 0.87. In the rainy season, when *G* is included (i.e., $H + LE + G$), the energy balance closure was approximately 0.53 ($R^2 = 0.81$, Fig. 11a). When *S* is included (i.e., $H + LE + S$), the correlation slightly decreases ($R^2 = 0.78$, Fig. 11b), but there was an improvement in energy balance closure (slope $= 0.63$). Including both *G* and *S* resulted in a significant improvement in the correlation between *Rn* and the sum of the fluxes ($R^2 = 0.80$, Fig. 11c), and in the energy balance closure (slope $= 0.66$). Despite the slight decrease in R^2, the inclusion of *S* contributed to a better closure of the energy balance, reducing the imbalance between incoming and outgoing energy. The improvement in energy balance closure was more pronounced during the dry season (Fig. 11d, e, f). The R^2 value was 0.84 when only *G* was considered, and increased to 0.87 with the inclusion of $G + S$ (Fig. 11f). The slope increased from 0.63 with *G* to 0.80 with $G + S$.

The residual average energy balance decreased (Table 5) from 37.51 Wm^{-2} (*G*) to 25.46 Wm^{-2} ($G + S$) in the wet season and from 20.77 Wm^{-2} (*G*) to 15.46 Wm^{-2} ($G + S$) in the dry season. Additionally, RMSE values were significantly reduced from 120.61 Wm^{-2} to 104.97 Wm^{-2} in the wet season and from 112.33 Wm^{-2} to 90.92 Wm^{-2} in the dry season, indicating improved prediction accuracy when both components ($G + S$) were incorporated into the model (Table 5).

The slope values (ranging from 0.53 to 0.80) and R^2 coefficients were within the ranges identified in 22 FLUXNET network sites[69], where slopes varied from 0.53 to 0.99, and R^2 from 0.64 to 0.96. With the inclusion of $G + S$, energy balance closure exceeded the average slope of 0.79 reported by Wilson et al.[69], as well as values for São Paulo (0.79 in February and 0.75 in August)[74]. Furthermore, incorporating $G + S$ improved the statistical metrics, suggesting that the *S* variable plays a critical role in energy balance closure, consistent with findings in the Amazon rainforest[30], where a reduction in imbalance and an improvement in energy balance closure (wet: 0.94 and dry: 0.89) were observed with the inclusion of canopy heat storage.

Summary and conclusions

In this study, we present results obtained from measurements conducted on the first tower dedicated to radiation and energy flux monitoring in an urban region of central Amazonia, located in Manaus, Amazonas, Brazil. Surrounded by the world's largest tropical rainforest, Manaus is a megacity and exhibits distinct and similar dynamics in energy and radiation exchanges compared to other densely populated cities without forest influence.

The reduced surface shortwave radiation, particularly during the wet season, may be associated with the high cloud cover over Manaus, contributing to significant variations between the wet and dry seasons (with maximum differences reaching 267 Wm^{-2}). The albedo showed statistically significant differences between seasons, being lower (higher) under wet (dry) conditions. This indicates that the proportion of reflected to incoming radiation shifts with reduced rainfall in the Amazon. Outgoing longwave radiation (LW_{out}) values were typical of urban surfaces, i.e., relatively high (especially in the dry season) compared to forested areas. This underscores how replacing forests with impermeable surfaces directly impacts ground surface temperatures. Net radiation values varied substantially between the wet (410 Wm^{-2}) and dry (565 Wm^{-2}) seasons in Manaus and were lower than those observed in adjacent and nearby forested areas. This reduction is explained by relatively higher LW_{out} values in urban regions than forests.

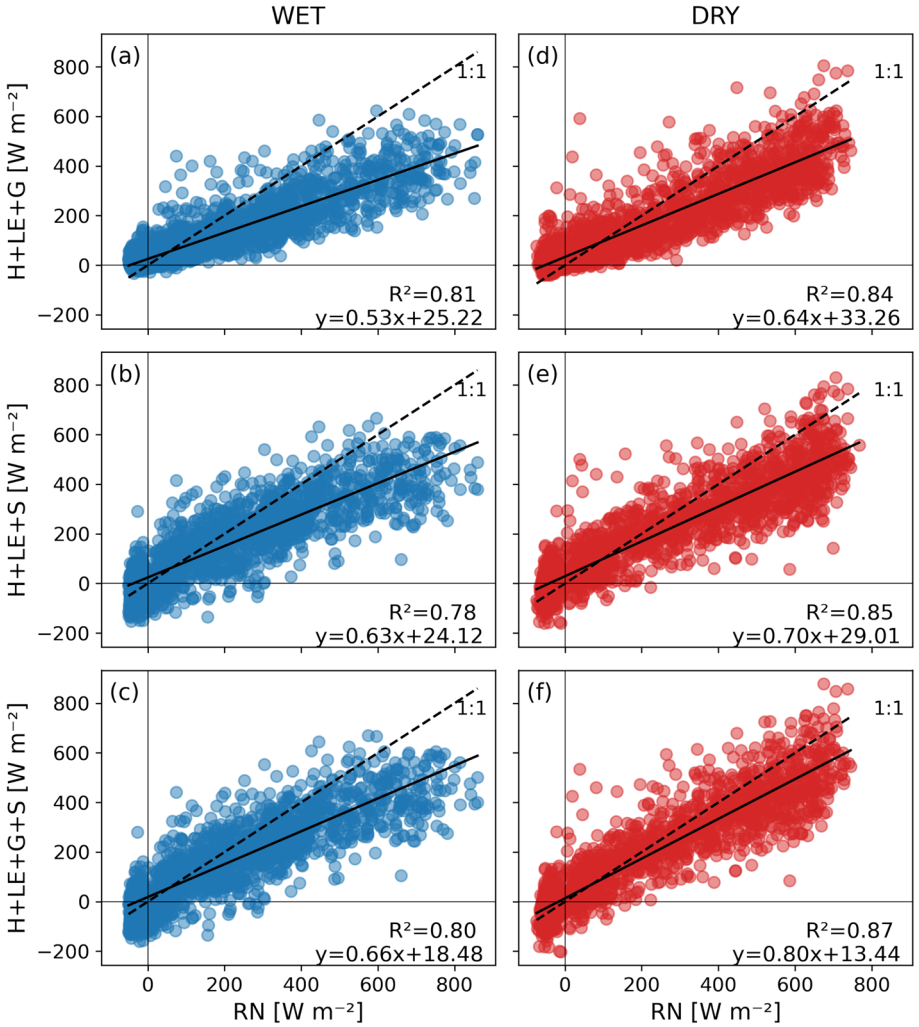

Fig. 11. Linear regressions between the sum of energy fluxes $H + LE + G$ and net radiation *Rn* (**a**, **d**); considering the inclusion of $+S$ (**b**, **e**); and the incorporation of all terms $G + S$ (**c**, **f**), for the wet (blue) and dry (red) seasons.

Variables	IMB	EBR	R^2	Intercept	Slope	RMSE
Wet						
G	37.51	0.72	0.81	25.22	0.53	120.61
G+S	25.46	0.80	0.80	18.48	0.66	104.97
Dry						
G	20.77	0.86	0.84	33.26	0.64	112.33
G+S	15.46	0.89	0.87	13.44	0.80	90.92

Table 5. Statistical metrics for energy balance closure, imbalance/residual (IMB), the closure method using the energy balance index (EBR); Coefficients (intercept, slope and R^2) of the linear regressions between the half-hour values of the sum of the energy fluxes $H + LE + G$ (or $H + LE + G + S$) and the *Rn*; and the statistical parameter RMSE (Root Mean Square Error) during the wet and dry seasons.

Regarding energy flux components, sensible heat flux exhibited the most pronounced seasonal variation (from 119 to 251 Wm^{-2} between wet and dry seasons), consistent with patterns observed in other urban areas. In contrast, latent heat flux showed minimal seasonal variation. This weak seasonality in *LE* is similar to forest regions in the Amazon and diverges from patterns in other cities, even those in tropical regions. It suggests that urban Manaus maintains relatively constant evaporation levels regardless of seasonal variations, pointing to other factors influencing *LE*, such as the directional variability of permeable surfaces (ranging from 9 to 31%, mostly vegetation) and horizontal moisture exchanges from external sources (e.g., the surrounding forest and

rivers). The seasonal variation in energy partitioning shows that *H* and *LE* play dominant roles in different seasons. During the wet season, *H* and *LE* are comparable at certain times of the day, with *LE* accounting for approximately 46% of *Rn*. In the dry season, *H* dominates, contributing 55% of *Rn*. This behavior indicates that in the dry season, the surface directs more energy into *H* (higher Bowen ratio), whereas in the wet season, the evaporative fraction increases, reflecting greater contributions from evaporation due to higher humidity.

Heat storage in the urban canopy is predominantly influenced by heat stored in building walls, accounting for 72% of storage during the wet season and 97% during the dry season. The inclusion of conductive heat storage terms (*S* and *G*) significantly improved energy balance closure in both seasons, particularly during the dry season. However, the main limitations of this study is the absence of estimates for anthropogenic heat and the thermal contribution of paved surfaces in the energy balance. Accurate quantification of anthropogenic heat in tropical cities like Manaus remains a challenge due to the heterogeneity of urban infrastructure and the scarcity of detailed data, particularly regarding energy consumption. Another significant issue in urban canyon studies is the accurate estimation of heat emitted/absorbed by paved surfaces, which was not directly addressed in this work. However, considering the substantial thermal interaction between streets and walls, allowing part of the energy absorbed by horizontal surfaces to be transferred to the walls, it is believed that the estimation of S, obtained from sensors installed on the walls, indirectly measures the heat emitted by the streets. Finally, although it was not directly assessed in this study, horizontal advection may also influence the observed flux patterns, particularly given the complex topography of the site. An analysis of the covariances between the horizontal wind component (u) and scalars (such as temperature) as a proxy indicated that, although a non-negligible horizontal turbulent heat flux ($\overline{u'\theta'}$) is observed throughout the day, especially in the early afternoon, its magnitude remains relatively small (approximately 50% lower) compared to the vertical component ($\overline{w'\theta'}$). This suggests that horizontal heat transport may contribute to the energy exchange, potentially associated with surface heterogeneities or local advection. However, the potential contribution of horizontal fluxes still requires further evaluation. For future studies, it would be important to obtain experimental data and adopt methods that allow for the direct estimation of heat storage in the urban volume, aiming to achieve a better representation of these energy fluxes in Amazonian urban environments.

The data presented here have significant implications for various areas of climate and environmental research, including the validation and calibration of urban models used in mesoscale simulations to investigate phenomena such as the UHI, the analysis of urban climate extremes, and the evaluation of greenhouse gas mitigation policies in urban contexts. Expanding similar studies to other urban centers in the Amazon is essential to provide a more detailed understanding of energy and radiation balances across regions with different types of land use and cover.

Data availability

The datasets used and/or analysed during the current study available from the corresponding author on reasonable request.

Received: 22 February 2025; Accepted: 11 September 2025
Published online: 21 October 2025

References

1. Nations, U. *World urbanization prospects: The 2014 revision* (United Nations, 2014).
2. Economic, U. N. D. o. & Affairs, S. Urban and rural population growth and world urbanization prospects. In *World Urbanization Prospects: The 2018 Revision*, 9–31 (United Nations, 2019).
3. Un-Habitat. *Cities and Climate Change: Global Report on Human Settlements 2011* (Routledge, London, 2011).
4. Oke, T. R. The distinction between canopy and boundary-layer urban heat islands. *Atmosphere* **14**, 268–277. https://doi.org/10.1080/00046973.1976.9648422 (1976).
5. Roth, M. Review of atmospheric turbulence over cities. *Q. J. Royal Meteorol. Soc.* **126**, 941–990. https://doi.org/10.1002/qj.49712656409 (2000).
6. Oke, T. R., Mills, G., Christen, A. & Voogt, J. A. Urban Heat Island. In *Urban Climates*, 197–237, https://doi.org/10.1017/9781139016476.008 (Cambridge University Press, Cambridge, 2017).
7. Barlow, J. F. Progress in observing and modelling the urban boundary layer. *Urban Clim.* **10**, 216–240. https://doi.org/10.1016/j.uclim.2014.03.011 (2014).
8. Oliveira, A. P. d. *et al.* Assessing urban effects on the climate of metropolitan regions of Brazil - preliminary results of the MCITY BRAZIL project. *Exploratory Environmental Science Research* (2020).
9. Feigenwinter, C., Vogt, R. & Christen, A. Eddy Covariance Measurements Over Urban Areas. In Aubinet, M., Vesala, T. & Papale, D. (eds.) *Eddy Covariance: A Practical Guide to Measurement and Data Analysis*, Springer Atmospheric Sciences, 377–397, https://doi.org/10.1007/978-94-007-2351-1_16 (Springer Netherlands, Dordrecht, 2012).
10. Baldocchi, D. D. & Meyers, T. P. Turbulence structure in a deciduous forest. *Bound. Layer Meteorol.* **43**, 345–364. https://doi.org/10.1007/BF00121712 (1988).
11. Moncrieff, J. B. et al. A system to measure surface fluxes of momentum, sensible heat, water vapour and carbon dioxide. *J. Hydrol.* **188–189**, 589–611. https://doi.org/10.1016/S0022-1694(96)03194-0 (1997).
12. Foken, T., Aubinet, M. & Leuning, R. The Eddy Covariance Method. In Aubinet, M., Vesala, T. & Papale, D. (eds.) *Eddy Covariance: A Practical Guide to Measurement and Data Analysis*, Springer Atmospheric Sciences, 1–19, https://doi.org/10.1007/978-94-007-2351-1_1 (Springer Netherlands, Dordrecht, 2012).
13. Cleugh, H. A. & Oke, T. R. Suburban-rural energy balance comparisons in summer for Vancouver, B.C. *Bound. Layer Meteorol.* **36**, 351–369. https://doi.org/10.1007/BF00118337 (1986).
14. Grimmond, C. S. B. The suburban energy balance: Methodological considerations and results for a mid-latitude west coast city under winter and spring conditions. *Int. J. Climatol.* **12**, 481–497. (1992).
15. Grimmond, C. S. B. & Oke, T. R. Comparison of Heat Fluxes from Summertime Observations in the Suburbs of Four North American Cities. *Journal of Applied Meteorology and Climatology* **34**, 873–889 (1995). Publisher: American Meteorological Society Section: Journal of Applied Meteorology and Climatology.

16. Moriwaki, R. & Kanda, M. Seasonal and diurnal fluxes of radiation, heat, water vapor, and carbon dioxide over a suburban area. *J. Appl. Meteorol. Climatol.* **43**, 1700–1710. https://doi.org/10.1175/JAM2153.1 (2004).
17. Ferreira, M. J., Oliveira, A. P. & Soares, J. Diurnal variation in stored energy flux in São Paulo city. *Brazil. Urban Climate* **5**, 36–51. https://doi.org/10.1016/j.uclim.2013.06.001 (2013).
18. Roth, M., Jansson, C. & Velasco, E. Multi-year energy balance and carbon dioxide fluxes over a residential neighbourhood in a tropical city. *Int. J. Climatol.* **37**, 2679–2698. https://doi.org/10.1002/joc.4873 (2017).
19. Cui, W. & Chui, T. F. M. Measurements and simulations of energy fluxes over a high-rise and compact urban area in Hong Kong. *Sci. Total Environ.* **765**, 142718. https://doi.org/10.1016/j.scitotenv.2020.142718 (2021).
20. Miao, S., Dou, J., Chen, F., Li, J. & Li, A. Analysis of observations on the urban surface energy balance in Beijing. *Sci. China Earth Sci.* **55**, 1881–1890. https://doi.org/10.1007/s11430-012-4411-6 (2012).
21. Shuttleworth, W. J. et al. Eddy correlation measurements of energy partition for Amazonian forest. *Q. J. Royal Meteorol. Soc.* **110**, 1143–1162. https://doi.org/10.1002/qj.49711046622 (1984).
22. Shuttleworth, W. J. Evaporation from Amazonian rainforest. *Proceedings of the Royal Society of London. Series B. Biological Sciences* **233**, 321–346, https://doi.org/10.1098/rspb.1988.0024 (1988).
23. Fitzjarrald, D. R., Stormwind, B. L., Fisch, G. & Cabral, O. M. R. Turbulent transport observed just above the Amazon forest. *J. Geophys. Res. Atmos.* **93**, 1551–1563. https://doi.org/10.1029/JD093iD02p01551 (1988).
24. Bastable, H. G., Shuttleworth, W. J., Dallarosa, R. L. G., Fisch, G. & Nobre, C. A. Observations of climate, albedo, and surface radiation over cleared and undisturbed amazonian forest. *Int. J. Climatol.* **13**, 783–796. https://doi.org/10.1002/joc.3370130706 (1993).
25. Sá, L. D. & d. A., Viswanadham, Y. & Manzi, A. O,. Energy flux partitioning over the Amazon forest. *Theor. Appl. Climatol.* **39**(1–16), 1988. https://doi.org/10.1007/BF00867653 (1988).
26. Araújo, A. C. *et al.* Comparative measurements of carbon dioxide fluxes from two nearby towers in a central Amazonian rainforest: The Manaus LBA site. *Journal of Geophysical Research: Atmospheres* **107**, LBA 58–1–LBA 58–20, https://doi.org/10.1029/2001JD000676 (2002).
27. Malhi, Y. et al. Energy and water dynamics of a central Amazonian rain forest. *J. Geophys. Res.: Atmos.* https://doi.org/10.1029/2001JD000623 (2002).
28. Rocha, H. R. et al. Seasonality of water and heat fluxes over a tropical forest in Eastern Amazonia. *Ecol. Appl.* **14**, 22–32. https://doi.org/10.1890/02-6001 (2004).
29. Randow, C. et al. Comparative measurements and seasonal variations in energy and carbon exchange over forest and pasture in South West Amazonia. *Theor. Appl. Climatol.* **78**, 5–26. https://doi.org/10.1007/s00704-004-0041-z (2004).
30. Michiles, A. A. d. S. & Gielow, R. Above-ground thermal energy storage rates, trunk heat fluxes and surface energy balance in a central Amazonian rainforest. *Agricultural and Forest Meteorology* **148**, 917–930, https://doi.org/10.1016/j.agrformet.2008.01.001 (2008).
31. Zeri, M. & Sá, L. D. A. The impact of data gaps and quality control filtering on the balances of energy and carbon for a Southwest Amazon forest. *Agr. Forest Meteorol.* **150**, 1543–1552. https://doi.org/10.1016/j.agrformet.2010.08.004 (2010).
32. Gerken, T. et al. Investigating the mechanisms responsible for the lack of surface energy balance closure in a central Amazonian tropical rainforest. *Agr. Forest Meteorol.* **255**, 92–103. https://doi.org/10.1016/j.agrformet.2017.03.023 (2018).
33. Restrepo-Coupe, N. et al. Understanding water and energy fluxes in the Amazonia: Lessons from an observation-model intercomparison. *Global Change Biol.* **27**, 1802–1819. https://doi.org/10.1111/gcb.15555 (2021).
34. Fisch, G. et al. The convective boundary layer over pasture and forest in Amazonia. *Theor. Appl. Climatol.* **78**, 47–59. https://doi.org/10.1007/s00704-004-0043-x (2004).
35. Carneiro, R. G. & Fisch, G. Observational analysis of the daily cycle of the planetary boundary layer in the central Amazon during a non-El Niño year and El Niño year (GoAmazon project 2014/5). *Atmos. Chem. Phys.* **20**, 5547–5558. https://doi.org/10.5194/acp-20-5547-2020 (2020).
36. Dias-Júnior, C. Q. *et al.* Intercomparison of Planetary Boundary Layer Heights Using Remote Sensing Retrievals and ERA5 Reanalysis over Central Amazonia. *Remote Sensing* **14**, https://doi.org/10.3390/rs14184561 (2022).
37. Brazilian Institute of Geography and Statistics (IBGE). *1980 Population Census: Preliminary Results*. General Census of Brazil 1980, 9 (IBGE, Rio de Janeiro, 1980).
38. Brazilian Institute of Geography and Statistics - IBGE. Manaus Data - 2010 Brazilian Census (2010).
39. Fisch, G. Climatic aspects of the Amazonian tropical forest. *Acta Amazonica* **20**, 39–48 (1990). Publisher: SciELO Brasil.
40. Souza, D. O. d. & Alvalá, R. C. d. S. Observational evidence of the urban heat island of Manaus City, Brazil. *Meteorological Applications* **21**, 186–193, https://doi.org/10.1002/met.1340 (2014).
41. Espinoza, N. d. S. *et al.* Assessment of urban heat islands and thermal discomfort in the Amazonia biome in Brazil: A case study of Manaus city. *Building and Environment* **227**, 109772, https://doi.org/10.1016/j.buildenv.2022.109772 (2023).
42. Krüger, E. et al. The impact of urbanization on heat stress in Brazil: A multi-city study. *Urban Climate* **53**, 101827. https://doi.org/10.1016/j.uclim.2024.101827 (2024).
43. Carvalho, D. L. R., SOARES, C. & SILVA, M. M. d. Identificação de Ilhas de Calor Urbana na Cidade de Manaus-AM. *Simposio Brasileiro de Sensoriamento Remoto* **16**, 874–881 (2013).
44. Santos, C. A. C. D. & Lima, J. R. A. Análise dos Efeitos da Expansão Urbana de Manaus-AM Sobre Parâmetros Ambientais Através de Imagens de Satélite (Analysis of the Urban Expansion Effects of Manaus-AM on Environmental Parameters through Satellite Images). *Revista Brasileira de Geografia Fisica* **6**, 001–014, https://doi.org/10.26848/rbgf.v06.1.p001-014 (2013).
45. Corrêa, P. B., Candido, L. A., Souza, R. A. F. d., Andreoli, R. V. & Kayano, M. T. Estudo do Fenômeno da Ilha de Calor na Cidade de Manaus/AM: Um Estudo a Partir de Dados de Sensoriamento Remoto, Modelagem e Estações Meteorológicas. *Revista Brasileira de Meteorologia* **31**, 167–176, https://doi.org/10.1590/0102-778631220150012 (2016). Publisher: Sociedade Brasileira de Meteorologia.
46. Monteiro, F. F., Gonçalves, W. A., Andrade, L. d. M. B., Villavicencio, L. M. M. & dos Santos Silva, C. M. Assessment of Urban Heat Islands in Brazil based on MODIS remote sensing data. *Urban Climate* **35**, 100726, https://doi.org/10.1016/j.uclim.2020.100726 (2021).
47. Farias, C. D. S. et al. *Estimation of Anthropogenic Heat Flux in a City in the Central Amazon* https://doi.org/10.2139/ssrn.4516056 (2023).
48. Hall, D. H. et al. Comparative study of energy balance in urban and forest areas in central Amazonia. *Ciencia e Natura* **45**, e80263. https://doi.org/10.5902/2179460X80263 (2023).
49. Shrivastava, M. et al. Urban pollution greatly enhances formation of natural aerosols over the Amazon rainforest. *Nature Commun.* **10**, 1046. https://doi.org/10.1038/s41467-019-08909-4 (2019).
50. Souza, C. M. *et al.* Reconstructing Three Decades of Land Use and Land Cover Changes in Brazilian Biomes with Landsat Archive and Earth Engine. *Remote Sensing* **12**, 2735, https://doi.org/10.3390/rs12172735 (2020). Number: 17 Publisher: Multidisciplinary Digital Publishing Institute.
51. MapBiomas. Mapbiomas project: Collection 7 of the annual land use and land cover maps of brazil (2022). Accessed on March 18, 2022, from https://brasil.mapbiomas.org/.
52. Rebmann, C. *et al.* Data Acquisition and Flux Calculations. In Aubinet, M., Vesala, T. & Papale, D. (eds.) *Eddy Covariance: A Practical Guide to Measurement and Data Analysis*, Springer Atmospheric Sciences, 59–83, https://doi.org/10.1007/978-94-007-2351-1_3 (Springer Netherlands, Dordrecht, 2012).

53. Fratini, G. & Mauder, M. Towards a consistent eddy-covariance processing: an intercomparison of EddyPro and TK3. *Atmospheric Measurement Techniques* **7**, 2273–2281, https://doi.org/10.5194/amt-7-2273-2014 (2014). Publisher: Copernicus GmbH.
54. Gash, J. H. C. & Culf, A. D. Applying a linear detrend to eddy correlation data in realtime. *Bound. Layer Meteorol.* **79**, 301–306. https://doi.org/10.1007/BF00119443 (1996).
55. Moncrieff, J., Clement, R., Finnigan, J. & Meyers, T. Averaging, Detrending, and Filtering of Eddy Covariance Time Series. In Lee, X., Massman, W. & Law, B. (eds.) *Handbook of Micrometeorology: A Guide for Surface Flux Measurement and Analysis*, Atmospheric and Oceanographic Sciences Library, 7–31, https://doi.org/10.1007/1-4020-2265-4_2 (Springer Netherlands, Dordrecht, 2005).
56. Vickers, D. & Mahrt, L. Quality Control and Flux Sampling Problems for Tower and Aircraft Data. *Journal of Atmospheric and Oceanic Technology* **14**, 512–526, (1997). Publisher: American Meteorological Society Section: Journal of Atmospheric and Oceanic Technology.
57. Wilczak, J. M., Oncley, S. P. & Stage, S. A. Sonic anemometer tilt correction algorithms. *Bound. Layer Meteorol.* **99**, 127–150. https://doi.org/10.1023/A:1018966204465 (2001).
58. Ibrom, A., Dellwik, E., Flyvbjerg, H., Jensen, N. O. & Pilegaard, K. Strong low-pass filtering effects on water vapour flux measurements with closed-path eddy correlation systems. *Agric. Forest Meteorol.* **147**, 140–156. https://doi.org/10.1016/j.agrformet.2007.07.007 (2007).
59. Ibrom, A., Dellwik, E., Larsen, S. E. & Pilegaard, K. On the use of the Webb–Pearman–Leuning theory for closed-path eddy correlation measurements. *Tellus B Chem. Phys. Meteorol.* **59**, 937. https://doi.org/10.1111/j.1600-0889.2007.00311.x (2007).
60. Fisch, G., Marengo, J. A. & Nobre, C. A. Uma revisão geral sobre o clima da Amazônia. *Acta Amazonica* **28**, 101–101, https://doi.org/10.1590/1809-43921998282126 (1998). Publisher: Instituto Nacional de Pesquisas da Amazônia.
61. Foken, T. *et al.* Post-Field Data Quality Control. In Lee, X., Massman, W. & Law, B. (eds.) *Handbook of Micrometeorology: A Guide for Surface Flux Measurement and Analysis*, Atmospheric and Oceanographic Sciences Library, 181–208, https://doi.org/10.1007/1-4020-2265-4_9 (Springer Netherlands, Dordrecht, 2005).
62. Oke, T. R., Mills, G., Christen, A. & Voogt, J. A. Energy Balance. In *Urban Climates*, 156–196, https://doi.org/10.1017/9781139016476.007 (Cambridge University Press, Cambridge, 2017).
63. Shahmohamadi, P., Che-Ani, A. I., Maulud, K. N. A., Tawil, N. M. & Abdullah, N. a. G. The Impact of Anthropogenic Heat on Formation of Urban Heat Island and Energy Consumption Balance. *Urban Studies Research* **2011**, e497524, https://doi.org/10.1155/2011/497524 (2011).
64. Gabey, A. M., Grimmond, C. S. B. & Capel-Timms, I. Anthropogenic heat flux: advisable spatial resolutions when input data are scarce. *Theor. Appl. Climatol.* **135**, 791–807. https://doi.org/10.1007/s00704-018-2367-y (2019).
65. Nunez, M. & Oke, T. R. The Energy Balance of an Urban Canyon. *Journal of Applied Meteorology and Climatology* **16**, 11–19, (1977). Publisher: American Meteorological Society Section: Journal of Applied Meteorology and Climatology.
66. Roberts, S. M., Oke, T. R., Grimmond, C. S. B. & Voogt, J. A. Comparison of four methods to estimate Urban heat storage. *J. Appl. Meteorol. Climatol.* **45**, 1766–1781. https://doi.org/10.1175/JAM2432.1 (2006).
67. Mauder, M., Foken, T. & Cuxart, J. Surface-energy-balance closure over land: A review. *Bound. Layer Meteorol.* **177**, 395–426. https://doi.org/10.1007/s10546-020-00529-6 (2020).
68. Sun, J., Massman, W. J., Banta, R. M. & Burns, S. P. Revisiting the Surface Energy Imbalance. *Journal of Geophysical Research: Atmospheres* **126**, e2020JD034219, https://doi.org/10.1029/2020JD034219 (2021).
69. Wilson, K. et al. Energy balance closure at FLUXNET sites. *Agric. Forest Meteorol.* **113**, 223–243. https://doi.org/10.1016/S0168-1923(02)00109-0 (2002).
70. Kljun, N., Calanca, P., Rotach, M. W. & Schmid, H. P. A simple parameterisation for flux footprint predictions. *Bound. Layer Meteorol.* **112**, 503–523. https://doi.org/10.1023/B:BOUN.0000030653.71031.96 (2004).
71. Collow, A. B. M., Miller, M. A. & Trabachino, L. C. Cloudiness over the Amazon rainforest: Meteorology and thermodynamics. *J. Geophys. Res. Atmos.* **121**, 7990–8005. https://doi.org/10.1002/2016JD024848 (2016).
72. Ferreira, M. J. et al. Radiation balance at the surface in the city of São Paulo, Brazil: diurnal and seasonal variations. *Theor. Appl. Climatol.* **107**, 229–246. https://doi.org/10.1007/s00704-011-0480-2 (2012).
73. Oke, T. R., Mills, G., Christen, A. & Voogt, J. A. Radiation. In *Urban Climates*, 122–155, https://doi.org/10.1017/9781139016476.006 (Cambridge University Press, Cambridge, 2017).
74. Ferreira, M. J. et al. Surface energy balance in a suburban area of the megacity of São Paulo - seasonal variation and closure. *Urban Climate* **56**, 102008. https://doi.org/10.1016/j.uclim.2024.102008 (2024).
75. Moore, C. J. & Fisch, G. Estimating heat storage in Amazonian tropical forest. *Agric. Forest Meteorol.* **38**, 147–168. https://doi.org/10.1016/0168-1923(86)90055-9 (1986).
76. Do Couto, E. V., Carletti, R., De Vries, W. T. & Durán-Díaz, P. Spatial and temporal effects of urban growth in Manaus: examining urban and periurban sprawl in the heart of the world's largest tropical rainforest, Brazil. In *Modern Cartography Series*, vol. 11, 409–428, https://doi.org/10.1016/B978-0-443-15832-2.00018-6 (Elsevier, 2024).

Acknowledgements

This work is part of the PhD dissertation of the first author in the Postgraduate Program in Climate and Environment (PPG-CLIAMB) of the National Institute for Amazonian Research (INPA) and the Amazonas State University (UEA) with financial support from the Foundation for Research Support of Amazonas (FAPEAM) (POSGRAD/FAPEAM). The authors acknowledge the IETÉ, R&D project carried out by INPA, in partnership with SAMSUNG Eletrônica da Amazônia, with funds provided under Federal Law No. 8,387/1991, in accordance with Article 39 of Decree No. 10,521/2020. The authors received funding from the National Council for Scientific and Technological Development (CNPq) (Processes 434176/2018-4); Coordination of Superior Level Staff Improvement (CAPES) (PROAP/PDPG); C. Q. D. J. acknowledges support from CNPQ (Processes 440170/2022-2, 406884/2022-6, 307530/2022-1); A.S. acknowledges support from Research Ireland through the Research Ireland Centre for Research Training in Machine Learning (18/CRT/6183); We would like to thank the Large Scale Biosphere-Atmosphere Program (LBA), coordenated by the National Institute for Amazon Researches (INPA), for the use and availability of data, for logistical support and infrastructure during field activities; Amazonas Military Fire Department (CBMAM); Climate Modeling Laboratory (LMC/INPA); and Micromet team of ATTO Project.

Author contributions

D.H.H. conceived the study, developed the methodology, conducted the investigation, performed formal analysis, supervised the research, wrote the original draft, validated the findings, and curated the data. L.A.C. contributed to conceptualization, provided resources, reviewed and edited the manuscript, managed the project, and secured funding. B.T.T.P. contributed to methodology, provided resources, reviewed and edited the manuscript, and participated in project administration. G.F. contributed to conceptualization, methodology, investigation,

and manuscript review. R.V.A. contributed to conceptualization and manuscript review. R.A.F.S. contributed to conceptualization and manuscript review. A.S. reviewed and edited the manuscript. A.V.G. contributed to methodology and provided resources. A.C.S.M. contributed to methodology and manuscript review. C.S.F. contributed to methodology and manuscript review. J.R.M. contributed to methodology and provided resources. J.J.M. contributed to methodology and provided resources. M.C.M. contributed to methodology and provided resources. M.J.M.M. contributed to methodology, manuscript review, and provided resources. R.C.F. contributed to methodology, validation, and provided resources. R.C.O. contributed to methodology and provided resources. T.L.X. contributed to methodology and provided resources. C.Q.D.J. contributed to conceptualization, methodology, investigation, resources, manuscript review, supervision, project administration, and validation. All authors reviewed the manuscript.

Funding

Authors did not receive any funding for this work.

Declarations

Competing interests

The authors declare no competing interests.

Additional information

Supplementary Information The online version contains supplementary material available at https://doi.org/10.1038/s41598-025-19952-1.

Correspondence and requests for materials should be addressed to C.Q.D.-J.

Reprints and permissions information is available at www.nature.com/reprints.

Publisher's note Springer Nature remains neutral with regard to jurisdictional claims in published maps and institutional affiliations.